Institut
de Ciències
Fotòniques

Neuron Guidance and Nano-Neurosurgery Using Optical Tools

Manoj V. Mathew

Barcelona, June, 2009

Universitat Politècnica de Catalunya

ICFO - Institut de Ciències Fotòniques

Chapter 8

Cloning *mnm-4(et4)* and *sa580* genes in *C. elegans*

8.1 Overview

The works described in this thesis, so far, has involved the use of optical tools to induce axon guidance and cell manipulation in neurons, as well as development of multimodal microscopy tools to study various biological structures. However some important questions like why axons respond to distantly placed light sources requires a better understanding of biology and biological tools, particularly molecular biology and genetics. With this idea in mind I spent five months in the group of Dr. Marc Pilon, in the department of cell and molecular biology in Gothenburg University, Sweden.

One of the main themes of the Pilon group's research has been the understanding of the development of pharyngeal neurons in *C.elegans* [228]. The group had previously isolated and mapped five novel mutations affecting the development of a specific pharyngeal neuron, namely the M2 motorneuron. These five mutations were designated *mnm-1* to *mnm-5*, where "mnm" stands for "M Neuron Morphology abnormal" .

Among these mutations the *mnm-4(et4)* mutation is of particular interest. In worms with this mutation the two M2 neurons were found to be twisted around each other. A detailed study revealed that this is a result of an overall twist in the pharynx of the worm itself in which these neurons are located. A similar twisted pharynx phenotype was also observed by another group (Peter Svoboda group, Karolinska Institute, Stockholm, Sweden) in a mutant dubbed *sa580*.

This chapter describes my efforts in cloning the gene in *mnm-4(et4)* and *sa580* causing the twisted pharynx phenotype and some studies related to their functions.

8.2 Introduction

The pharynx is a prominent feature in the head of *C.elegans* that pumps rhythmically to suck bacteria into the lumen and grind them for digestion. It can be subdivided into six sections, which are, from anterior to posterior, the buccal cavity, procorpus, metacorpus (anterior bulb), isthmus, terminal bulb and pharyngeal-intestinal valve [147]. It is primarily a muscular structure with epithelial as well as gland cells. The pharynx is

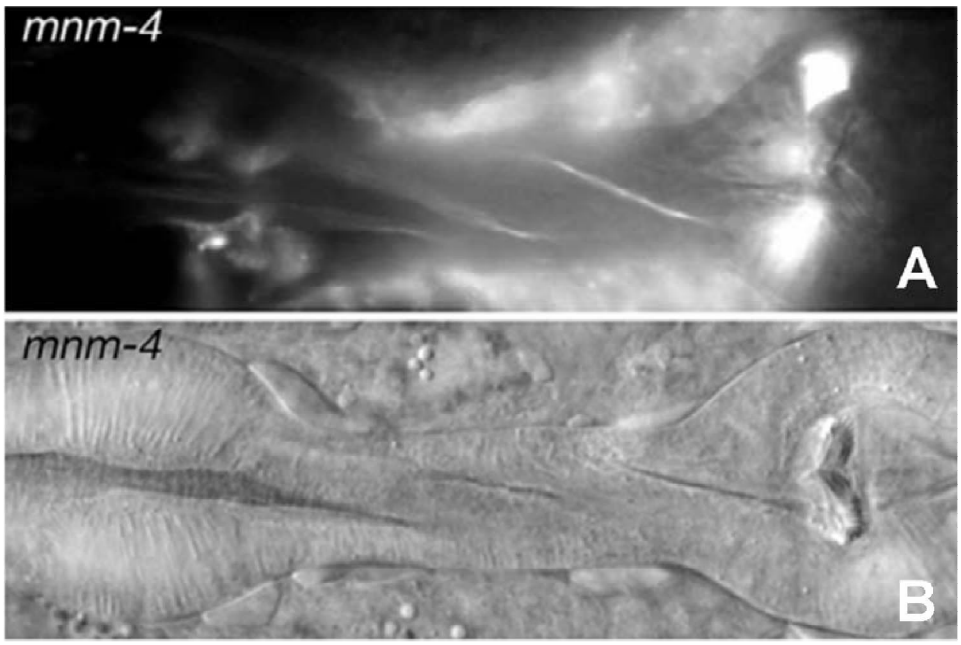

Figure 8.1: (a):The epi-fluorescence image of the twisted M2 neurons in *mnm-4(et4)* mutant background with a GFP integrated array (b) the normaski image of the twisted pharynx [228].

composed of eight layers of muscles (pm1-8) separated by structural marginal cells (mc1-3) [147]. These are arranged with three-fold rotational symmetry. The pharynx has its own nervous system consisting of 20 neurons that forms an almost complete sub-network.

Several *C.elegans* mutants show the twisted pharynx phenotype. In a screen for defects in the shape of hermaphrodite gonads the mutants *mig-4* and *dig-1* were isolated [229; 230] and these also have a twisted pharynx. Similarly the uncoordinated mutant *unc-61* also has a twisted pharynx [231]. The *mnm-4(et4)* mutant was isolated in a screen for abnormal morphology of the M2 pharyngeal neurons. The M2 neurons showed a twisted phenotype which was subsequently attributed to an overall twist in the whole pharynx [228]. Figure 8.1 shows the epi-fluorescence image of the twisted M2 neurons in *mnm-4(et4)* mutant background with a GFP integrated array (a) and the normaski image of the twisted pharynx (b) [228]. A similar observation was made in screen for abnormal amphid sensory neuron dendrites. The mutant *sa580* showed twisted amphid sensory neuron dendrites, again due to an overall twist in the pharynx. Figure 8.2 shows volume rendering of image stacks obtained at consecutive focal planes (imaged using Second Harmonic Generation (SHG) microscopy) of isthmus of the pharynx of wild type N2 (Figure 8.2A), *mnm-4(et4)* (Figure 8.2B) and *sa580* (Figure 8.2C) strains.

mnm-4(et4) is semi-dominant: the heterozygous with a wild type allele shows a weak twist. In contrast, the *sa580* allele is recessive: the heterozygous genotype has no twist.

8.2.1 Properties of the twisted pharynx

The pharyngeal twist is first visible post-embryonically and increases during development throughout the larval stages [232]. When looking along the anterior-posterior axis

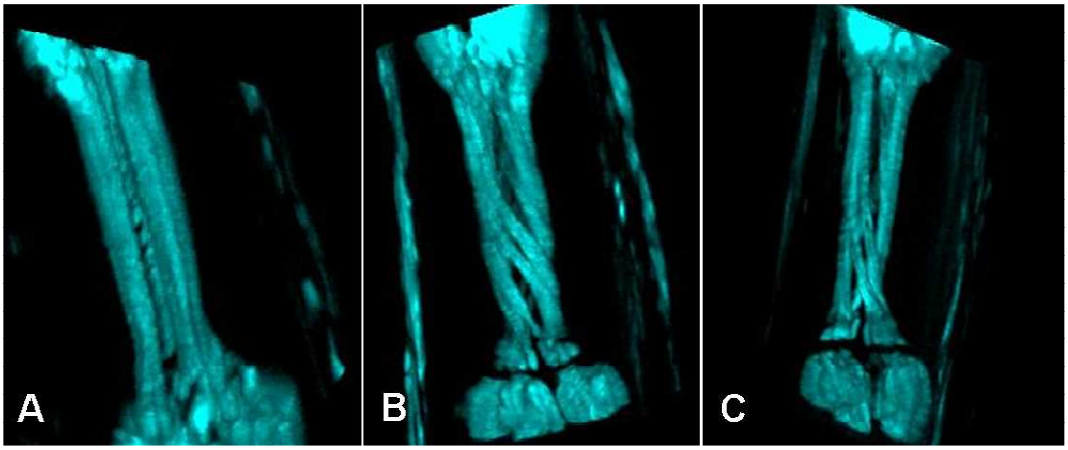

Figure 8.2: Volume rendered image stacks obtained at consecutive focal planes imaged using Second Harmonic Generation (SHG) microscopy of the isthmus of *C.elegans* pharynx. (A):wild type N2; (B): *mnm-4(et4)* and C: *sa580.* (Images obtained using the multimodal optical workstation).

pharynges of both *mnm-4(et4)* and *sa580* have a left-handed (counter-clockwise) twist. The twisting force is probably intrinsic to the pharynx since twisted pharynges when dissected out and allowed to relax in an isotonic medium retain their twist, whereas dissected pharynges of wild type worms donot twist [6].

The twisted pharynges are fully functional. In a bead intake assay animals with twisted pharynges performed as well as the wild type worms. This argument was further strengthened by electropharyngeograms, which showed no apparent difference in the pharyngeal membrane potential of *mnm-4(et4)* worms and wild type worms [232].

The basal surface of the pharynx is covered by a thick basal lamina and four rows of acellular tendinous organs composed of hemicentin and fibulin. The number and thickness of tendons was the same in wild-type and the mutants. However these tendons are pulled by the twist resulting in a spiral-like configuration when viewed along the anterior-posterior axis. Thus the whole pharynx, including its basal lamina to which the tendons are attached, is twisted in mutants [232].

Actin filaments form important radial cytoskeletal structures within the pharyngeal muscles cells. Using phalloidin as a staining reagent, it was found that these actin arrays are significantly longer in *mnm-4(et4)* than in N2 wild type worms. This is interesting since misregulation of filament length in growing pharyngeal muscles may be a cause of twisting: long actin filaments may be accommodated by twisting the pharynx. Alternatively, longer actin filaments could merely be a consequence of the twisted shape [232].

The force that causes twist in pharynges likely increases or is constantly applied through the larval developmental stages. The lack of twisting in L1 larvae is not due to the negation of an already existing twisting force by the attachment of the pharynx to the surrounding tissue, but due to the altogether lack of a twisting force in L1 stage. This was demonstrated by introducing the *mnm-4(et4)* mutation into *pha-1* genetic background. In the *pha-1* the connection of the pharynx with the buccal cavity fails during early L1 stage at the level of the arcade cells, leading to a Pun (Pharyngeal Unattached)

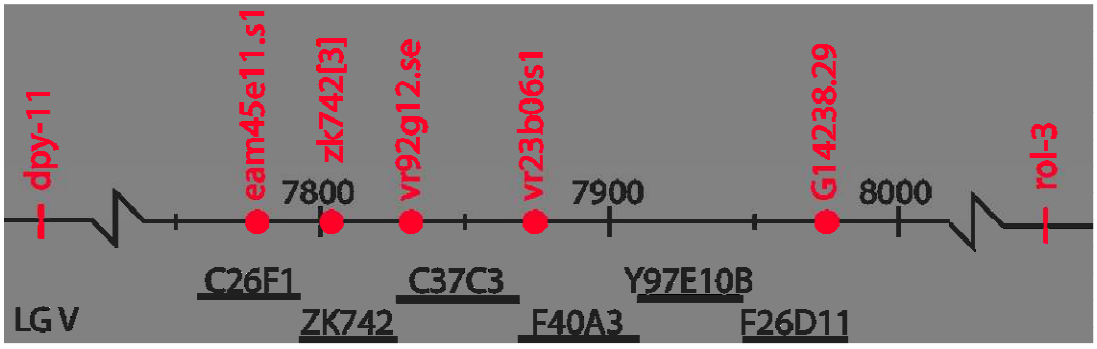

Figure 8.3: (Region in LGV to which the *mnm-4(et4)* mutation was mapped and the cosmids that span the region of interest

phenotype. No twisting could be detected in Pun-pharynges in L1 larvae of either the *pha-1* single mutant or in the *pha-1*;*mnm-4(et4)* double mutant [232].

Vigorous pharyngeal motions that accompany molting are not responsible for the twisting force since no sudden increase in twist is produced upon molting. This result also suggests that the pharyngeal cuticle is not directly restraining an intrinsic twist [232].

8.2.2 Likely causes of the twisted pharynx phenotype

As the pharynx grows there is no cell replacement, however actomyosin filaments must be continuously added to the pharyngeal muscle. This requires a reorganization of the cytoskeletal anchorage points to the extracellular matrix to accommodate growth. Hence a likely cause of the twisting phenotype is a bias in the repositioning of actin binding sites as that radial array grows [6]. The mutations that affect pharyngeal twist may affect the proteins required for actin anchorage, either at the basal lamina, or at the pharyngeal cuticle. *sa580* have left handed twist and *dig-1*, *mig-4*, and *sax-7* mutants produced a mixture of right- and left-handed twists and with a 25-30% penetrance. Hence there seems to be a chiral bias in mispositioning of cytoskeletal elements, that lead to the pharyngeal twist [232].

The *dig-1* and *sax-7* mutations affect adhesion molecules, and *unc-61* affects a cytoskeleton organizing septin. All the three molecules are expressed in the pharynx. Hence it seems very likely that the twisted pharynx may result from defects in ECM or cytoskeletal attachment points, or in interface structures by which ECM and cytoskeleton are connected [232].

8.2.3 Gene mapping and rescues to locate the mutation

Previous efforts in the Pilon group had mapped the *mnm-4(et4)* mutation to a region that was to the right of *dpy-11* and to the left of *rol-3* on the chromosome LG V. Figure 8.3 illustrates this region.

This region is covered by six cosmids (C26F1, ZK742, C373, F40A3, Y97E10B and F26D11). When tested in pairs ZK742 + C373 showed appreciable amounts of rescue. The *ppn-1* gene (*C.elegans* equivalent of the drosophila Papilin gene) has it promoter region within the cosmid ZK742 and the coding region within C373. *ppn-1* codes for a secreted

Extra Cellular Matrix (ECM) protein. Hence mutations in this gene could possibly create a twisted pharynx phenotype (from the arguments presented in section 8.2.2). Hence *ppn-1* was considered as the possible target for the mutation in *mnm-4(et4)*. Since the *sa580* causes the same phenotype, as *mnm-4(et4)*, and both mapped to similar regions, it was considered very likely that *mnm-4(et4)* and *sa580* are mutant alleles of the same gene.

8.3 Aims of the present work

1. Confirm that the mutation in *mnm-4(et4)* and *sa580* is indeed in the gene *ppn-1* and locate the mutation within the gene by sequencing it. This needs to done in five steps each for *mnm-4(et4)* and *sa580*, by PCR amplification of 5x 4kb (ppn-1 gene is about 20KB) fragments using a high-fidelity enzyme, subcloning the amplified fragments into the pCR®II Blunt Topo vector, purifying the resulting plasmids and shipping them to Eurofinn MWG together with sequencing primers for sequencing.
2. Study some functions of the twisted pharynges in the strains *mnm-4(et4)* and *sa580*.

8.4 Materials and Methods

8.4.1 Polymerase Chain Reaction (PCR)

Polymerase chain reaction (PCR) allows selective amplification of a chosen region of a DNA molecule, generating millions or more copies of the selected DNA fragment. The method relies on a thermal cycling process with cyclic heating and cooling that repeat the processes of DNA melting and enzymatic replication. A region is selected by defining the sequences at the borders of the region. Two short oligonucleiotides called primers, hybridize to the DNA molecule, one to each strand. These primers delimit the region that will be amplified [233]. As PCR progresses, the DNA generated is itself used as a template for replication, which results in a chain reaction where the DNA template is exponentially amplified. Ideally the fragment to be amplified by standard PCR techniques should be less than 1Kb. Fragments of around 4kb can be amplified using high fidelity polymerase enzymes.

The following reagents are required for PCR:

DNA polymerase- A thermostable DNA polymerase enzyme catalyzes the template dependent synthesis of DNA [234]. The most commonly used is the Taq DNA polymerase isolated from *T. aquaticus* thermophilic archea bacteria, which can with stand very high temperatures. However amplifications of DNA fragments greater than 1000 base pairs requires the use of a high fidelity enzyme, which are usually genetically engineered. Such an enzyme (Pfu Ulra, High-Fidelity DNA polymerase, Stratagene, USA) was used in the present work.

Two Primers: The primers act as initiators of the DNA synthesis reaction. These primers need to be complementary to the sequences at the ends of the target region on the template DNA molecule. One of the primers hybridizes to the 3' end in the region of interest in one strand of the DNA molecule and the other primer hybridizes to the 3' end of the complementary strand. The 3' ends of the primers hence point towards each other [233]. The length of the primers is critical. If they are too short they may hybridize to non-specific locations, however if they are too long hybridization takes a longer time, thus

decreasing efficiency of PCR.

Deoxynucleoside triphosphates (dNTPs)- These are the building blocks from which the DNA polymerases synthesizes new DNA strands. The typical PCR reaction contain equimolar amounts of dATP, dTTP, dCTP and dGTP.

Divalent Cations- Divalent cations like Mg^{++} are often required to increase the efficiency of the PCR reaction. These ions affect primer annealing and temperature denaturation, as well as enzyme activity and fidelity. Excess Mg^{++} however results in accumulation of non-specific amplification products.

Buffer to maintain pH- The buffer provides a suitable chemical environment for optimum activity and stability of the DNA polymerase. Usually a Tris-Cl buffer adjusted to a pH between 8.3 and 8.8 at room temperature is included in standard PCRs. During the extension phase of the PCR when the temperature is around 72^0C, the pH drops down to around 7.2 [234].

Template DNA- Contains the DNA region to be amplified.

The PCR is commonly carried out in a thermal cycler in reaction volumes of 10–200μl in small reaction tubes (0.2–0.5ml volumes). The thermal cycler heats and cools the reaction tubes to achieve the temperatures required at each step of the reaction (see below). Most thermal cyclers have heated lids to prevent condensation at the top of the reaction tube.

The following steps are involved in PCR:

1. *Initialization step*: This step consists of heating the reaction to a temperature of 94–96^0C, which is held for 1-9 minutes. It is only required for DNA polymerases that require heat activation by hot-start PCR.

2. *Denaturing*: The PCR mix is heated around 94^0C for 20–30 seconds, to melt the DNA template and primers by breakage of the hydrogen bonds that hold together the two strands of double stranded DNA molecule. This denatures the DNA and yields single strands of DNA.

3. *Annealing step*: The reaction mixture is cooled down to 50–65^0C for 20–40 seconds. The two strands could join back together at this temperature, however an excess of primers in the reaction mixture prevents this and allows annealing of these primers to the single-stranded DNA template [233]. The annealing temperature depends on the primers used. The following equation is usually used to calculate the annealing temperature:

$$T_m(^0C) \sim 2(N_A + N_T) + 4(N_G + N_C) \tag{8.1}$$

   Where N equals the number of primer Adenine (A), Thymine (T), Guanine (G) or Cytosine (C).

   Typically the annealing temperature is about 3–5 degrees below the T_m of the primers used. Stable DNA-DNA hydrogen bonds are only formed when the primer sequence very closely matches the template sequence. The polymerase binds to the primer-template hybrid and begins DNA synthesis.

4. *Extension/elongation step*: The temperature at this step is raised to around 72^0C . This value however depends on the DNA polymerase used. The polymerase attaches

to one end of each primer and synthesizes new strands of DNA complementary to the template. This is done by the addition of dNTPs that are complementary to the template in 5' to 3' direction, condensing the 5'-phosphate group of the dNTPs with the 3'-hydroxyl group at the end of the nascent (extending) DNA strand. The extension time depends both on the DNA polymerase used and on the length of the DNA fragment to be amplified. At each extension step, the amount of DNA target is doubled, leading to exponential (geometric) amplification of the specific DNA fragment.

5. *Cycling*: The steps 2–4 are repeated 20–40 times amplifying exponentially the amount of DNA fragments in each reaction step. The products of one step act as templates for the next.

6. *Final elongation*: This single step is occasionally performed at a temperature of 70–74^{0}C for 5–15 minutes after the last PCR cycle to ensure that any remaining single-stranded DNA is fully extended.

7. *Final hold*: This step at 4–15^{0}C for an indefinite time may be employed for short-term storage of the final reaction.

In the present work the following procedure was adopted for amplification of chosen DNA fragments:

The DNA template was obtained by lysis of a single *C.elegans* worm with the required genotype (*mnm-4*(*et4*) or *sa580*) using the Single Worm Lysis Buffer (SLWB) (See appendix E for protocol). After transferring the worm to a PCR reaction tube of 0.2ml, with 2μl of SLWB, the following temperature cycling program was used and lysis carried out in a PCR thermal cycler:

1. T=60^{0}C for 1 hour
2. T=95^{0}C for 15 min
3. T=4^{0}C forever

Once the worm was lysed, the PCR reaction mix (See appendix E for protocol) was added to the reaction tube and subjected to the following thermal cycling program in the thermal cycler:

1. T=95^{0}C for 1 hour (Initiation)
2. T=95^{0}C for 30 sec (Denaturing)
3. T=Tm^{0}C for 30 sec (Annealing)
4. T=72^{0}C for 5 mins (Elongation)
5. Goto 2 Rep 35 (Cycling)
6. T=72^{0}C for 5 mins (Final Elongation)

7. T=4^0C forever (Hold)

The target gene (*ppn-1*) is about 20KB in length. The amplification of the entire gene was done in fragments of 4KB each in 5 PCR reactions. This was done both for *mnm-4(et4)* and *sa580*. The 5 fragments were named ppn1_1 to ppn1_5. A total of 10 DNA fragments were hence amplified (five each for *mnm-4(et4)* and *sa580*). Table 8.1 gives the list of primers and annealing temperatures for the PCR amplification of each of the five fragments.

Table 8.1: Primers used in PCR amplification

Gene Fragment	Primers	Annealing Temperature (T_m)
ppn1_1	5‘-TAT CGG TCG TCG CAG GAC CT-3‘ 5‘-CAA GTC CGT TGC TGC AAG GT-3‘	55^0C
ppn1_2	5‘-CCA AAC TTT CTT TCC CGA AG-3‘ 5‘-CCG AAG TTG AAT TCT CCG GT-3‘	53^0C
ppn1_3	5‘-TGC GTT GAC TCT GAG TTC GGA-3‘ 5‘-CGA CGA CTA TGG GCG AAG GA-3‘	55^0C
ppn1_4	5‘-CCT CTT TCC CAG GAA ATC CA-3‘ 5‘-ATA CAC AAC GGG TAT GGT GGA-3‘	55^0C
ppn1_5	5‘-TCC GAT CGT TGC TCC ACG GT-3‘ 5‘-GGA AAA AGA GAT CTC GCA ATG GA-3‘	57^0C

8.4.2 Agarose Gel Electrophoresis

Agarose gel electrophoresis uses a agarose gel and electric current to separate DNA, or RNA by size. These molecules are negatively charged, hence when allowed to drift in an electric field they move towards the anode. The velocities at which the molecules drift depend on their mass. Massive molecules (more base pairs) drift slower than lighter ones, enabling gel electrophoresis to separate DNA molecules based on their mass into bands.

The electrophoresis is carried out in a tank with an agarose gel tray. The gel is prepared by boiling about 100ml of 0.7–4% solution of agar in the electrolytic buffer TBE (Tris-Borate-EDTA) with few microliters of Ethidium Bromide (EtBr: final concentration 5ng/ml). The distance between DNA bands of a given length is determined by the percentage of agarose in the gel. In general lower concentrations of agarose are better for larger molecules because they result in greater separation between bands that are close in size. EtBr is a dye that fluoresces when bound to DNA and exposed to UV light. The warm agar solution is poured in to the electrophoresis tank. A set of combs are placed dipped in the solution. When the solution solidifies into a gel, the combs are removed out living behind wells into which the DNA solutions can be loaded.

The gel tray is immersed into the electrophoresis tank with TBE buffer. A DNA ladder solution is loaded into the first well. A DNA ladder is a defined solution of DNA molecules of different lengths, but whose lengths are known. It acts as a reference to estimate the size of unknown DNA molecules. When run alongside the DNA solution to be tested/separated, the bands produced by the solution to be tested can be compared

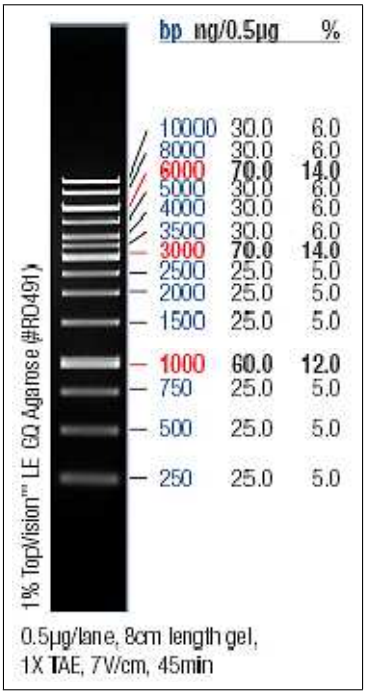

Figure 8.4: Fermentas gene ruler bands when run on a 1% agarose gel

to the ones in the lane with the DNA ladder. The DNA solutions to be tested/separated along with a negatively charged loading buffer are loaded into wells adjacent to the wells with the DNA ladder. Loading buffers commonly contain Ficol 400 which makes the sample denser than water, and allows it to be loaded into the wells.

Once the gel is loaded an electric field of about 5–8 volt/cm is applied to the tanks with the help of electrodes attached to the tank. The DNA moves toward the positive anode due to the negative charges on its phosphate backbone. Each well in the tray provides a separate track for electrophoresis. The DNA run down the track from the well and get separated according to mass and form distinctly visible bands. The progress of the process is made visible by the dyes in the loading buffer. Once the process is completed the bands can be observed under an UV lamp and photographed using a CCD camera.

Gel electrophoresis was utilized to check if the PCR reactions described in section 4.1 have worked fine and to separate out the amplified DNA. This was done by loading about 30μl of the PCR product along with a loading dye in a 1% agarose gel and running the electrophoresis with about 90 Volts applied across the electrodes for about 45mins, alongside a 1Kb Fermentas gene ruler solution. Figure 8.4 shows the bands obtained with this gene ruler when running it on a 1% agarose gel. A successful PCR reaction shows up as a band alongside the 4Kb band in the gene ruler. This band in the agarose gel was cut out and purified to extract the amplified DNA.

8.4.3 Extracting DNA by gel purification

Purification of DNA from excised gel band was performed using the QIAGEN QIAquick Gel Extraction kit. There are a set of buffers and reagents provided with the kit to help

completion of the process quite easily and quickly. The excised gel is first dissolved by incubating it in a buffer at 50^0C for about 10mins. Isopropanol is subsequently added to the solution to increase the yield. The solution is subsequently centrifuged in a specialized column. This column is the key component of the kit. The column has a special silica matrix that adsorbs DNA in the presence of high concentration of chemotropic salts, which are present in the buffer used to dissolve the gel. The buffer also provides the ideal pH conditions that help efficient binding of DNA to the matrix. While the DNA binds to the column the impurities pass down the column and are discarded. The contents are subsequently washed with a wash buffer and centrifuged to remove and residual impurities especially slats, while the DNA remains bound to the silica membrane. Any residual wash buffer is removed by an additional centrifugation step.

The bound DNA is subsequently eluted out by addition of an elution buffer and centrifugation. Usually 30-50μl of 10mM Tris is used as the elution buffer. The elution efficiency is strongly dependent on the salt concentration and pH of the elution buffer. A basic pH of around 8.5 is required for efficient elution and this pH is provided by the elution buffer. Once the DNA extraction is completed, the solution is checked for presence of DNA by gel electrophoresis.

8.4.4 Cloning the DNA fragments into plasmid vector

Plasmids are circular molecules of DNA that lead an existence independent of the chromosomal DNA in bacterial cells. They mostly carry one or more genes and are capable of replicating independently of the chromosomal DNA. Plasmid replication is usually carried out using the host cell's own DNA replicating mechanism; however larger plasmids carry genes that code for special enzymes that are specific for plasmid replication [233]. An important class of plasmids are the Resistance plasmids that confer the host bacteria resistance to antibacterial agents like Ampicillin or Kanamycin.

An important use of plasmids in molecular biology has been as vectors for the cloning of DNA fragments of interest into such plasmids, creating recombinant plasmid DNA. The DNA fragment that gets inserted into the plasmid is called an insert. Among other advantages it helps amplify these fragments by inserting these plasmids into bacteria and simply allowing the bacteria to multiply. The plasmids naturally multiply with the bacteria, amplifying the inserts contained within it.

Cloning of DNA fragments into plasmids is carried out in several steps. Initially the plasmid is cleaved at a single position to open up the circle, so that the DNA fragment (insert) can be inserted. This process is carried out using restriction endonucleases, that recognize specific sites in the plasmid and cleaves it. Most restriction endonucleases make a simple double stranded cut in the middle of the recognition sequence, resulting in a blunt or flush end [233]. However some restriction enzymes, cut the two strands of the DNA differently. The cleavage is staggered by two or four nucleotides, so that the resulting DNA fragments have short single stranded overhangs at each end. These are called sticky or staggered ends [233].

Once the plasmid DNA is cut open by the restriction enzyme, each end of the insert of interest is joined to one end of the cut plasmid DNA, forming a recombinant plasmid DNA. The joining together is done by a process called ligation. The process is catalyzed by the enzyme DNA ligase. This enzyme occurs naturally and helps in repairing broken DNA. If the restriction enzyme used, produced a blunt end, the insert has two possible

orientations in which it can gets ligated to the plasmid. However if the restriction enzyme produces a sticky end, the insert can get ligated only in one orientation, like a key getting inserted into a lock. In this case the insert too needs sticky ends; complementary to the ones on the plasmid.

In the present work the pCR®II Blunt TOPO cloning kit (Invitrogen, USA) was used for cloning the 10 DNA fragments (PCR products) (see section 8.4.1), creating 10 recombinant plasmids. The Zero Blunt TOPO cloning kit works differently from the conventional cloning technique described above using restriction enzyme and DNA ligase. Instead, this kit uses Topoisomerase I, that carries out both the functions (cleaving of the vector and ligation to the insert) in one go.

Topoisomerase I, is obtained form the Vaccinia Virus. It binds to double stranded DNA at specific sites and cleaves the phosphodiester backbone after the 5'-CCCTT in one strand. The energy form the broken phosphodiester backbone is conserved by formation of a covalent bond between the 3' phosphate of the cleaved strand and a tyrosine residue (Tyr-274) of topoisomerase I. The end result of this cleaving process is a plasmid DNA with toposiomerase bond to both the cleaved ends, at the strand with 3' phosphate. The 5' hydroxyl groups of the other DNA fragments (inserts) of interest attack this bond and release the topoisomerase, getting themselves bonded to the strand with the 3' phosphate in one end of the cleaved plasmid. The complementary strand of the insert which has the 5' hydroxyl group at the other end similarly binds to the 3' phosphate in the second end of the cleaved plasmid. This process effectively inserts the DNA fragment into the plasmid.

The insertion is carried out by simply incubating the required DNA fragments at room temperature with the pCR®II Blunt Topo vector together with a salt solution (See appendix E for detailed protocol). The kit provides the plasmid vector linearized with Vaccina virus DNA topoisomerase I covalently bound to the 3' end of each plasmid DNA strand. The plasmid has been so designed that the plasmids that donot get ligated with the DNA fragments kill the host cell upon transformation. Hence after transformation only those cells survive that have taken up the recombinant plasmid.

Transformation was carried out by incubating at 37^0C the recombinant plasmids with chemically competent *E.coli* bacterial cells and SOC medium provided with the kit. Competent cells have the ability to take up extracellular DNA from its environment. Hence when incubated with recombinant plasmid DNA they take up the plasmid and these plasmids get incorporated into the bacterial system. As the bacteria divide and multiply the recombinant plasmid get multiplied too.

The plasmid confers the transformed bacteria resistance to the antibiotic kanamycin. The transformed cells were plated onto LB agar plates with 50μg/ml kanamycin. Only those bacteria that have taken up the recombinant plasmid grow on these plates. The plates were incubated overnight at 37^0C to obtain bacterial colonies. Once bacterial colonies were obtained, four colonies were individually picked to inoculate 4 tubes containing 10ml LB liquid with 50μg/ml kanamycin and incubated at 37^0C overnight. Hence for each plasmid created, 4 tubes of bacterial cultures were obtained with bacteria seeded from 4 different colonies.

Minipreps were prepared form these tubes and plasmid DNA extracted and verified by digestion using restriction enzymes and subsequent gel electrophoresis (see Sections 8.4.5 and 8.4.6 for details).

The table 8.2 gives the details of recombinant plasmids created as part of this work.

Since the PCR products have blunt ends they have two orientations in which they could be inserted into the plasmid. The two possible orientations were designated a and b. The orientation is also indicated in the table 8.2.

Table 8.2: Details of recombinant plasmids created

Plasmid	*C.elegans* Strain	*ppn-1* Fragment	Orientation
pQC09.1a	*sa580*	ppn1_1	a
pQC09.2a	*sa580*	ppn1_2	a
pQC09.3bb	*sa580*	ppn1_3	b
pQC09.4b	*mnm-4(et4)*	ppn1_4	b
pQC09.5b	*mnm-4(et4)*	ppn1_5	b
pQC09.6a	*sa580*	ppn1_4	a
pQC09.7a	*sa580*	ppn1_5	a
pQC09.8a	*mnm-4(et4)*	ppn1_1	a
pQC09.9b	*mnm-4(et4)*	ppn1_3	b
pQC09.10a	*mnm-4(et4)*	ppn1_2	a

8.4.5 Making minipreps (Extraction of plasmid DNA)

For each plasmid created a miniprep was made for each of the four bacterial cultures (see section 8.4.4). This was done using the QIAprep Miniprep Kit (QIAGEN, USA). The miniprep procedure is based on alkaline lysis of bacterial cells followed by adsorption of DNA into a silica matrix in the presence of high concentration of salt.

In the initial step bacterial culture is centrifuged and the supernatant removed. The bacterial pellet is subsequently resuspended in a buffer and lysed by the addition of an alkaline lysis buffer. This process lyses the bacteria. Subsequently the lysate is neutralized and adjusted to high salt binding conditions by the addition of a neutralization buffer and centrifuged. This precipitates the SDS that was used in the buffer for cell lysis. The rest of the process is similar to the process explained in section 8.4.3. The supernatant is subsequently transferred to a specialized column with a silica matrix and centrifuged. The high salt concentration in the neutralization buffer helps binding of plasmid DNA to the silica membrane. The flow through is discarded. The high concentration of salts is removed by centrifugation after addition of a wash buffer. The plasmid DNA remains bound to the membrane. Any residual wash buffer is removed by an additional centrifugation step. Subsequently the plasmid DNA bound to the silica membrane is eluted out by centrifugation with 50μl of elution buffer.

For each plasmid four minipreps were created: one for each of the four bacterial cultures.

8.4.6 Digestion with restriction enzymes

A small amount of the extracted plasmid DNA from each of the four mininpreps was digested using specific restriction enzymes and subsequently analyzed by gel electrophoresis. This process is required to determine which of the four bacterial cultures had taken up the right plasmid and also to determine the orientation in which the insert (PCR product) got inserted in the plasmid. A restriction enzyme or restriction endonuclease cuts

DNA at specific recognition nucleotide sequences known as restriction sites. Depending on the restriction enzyme used the plasmid DNA gets cleaved at various locations specific to the plasmid under consideration as well orientation in which the DNA fragment (PCR product) got inserted into the plasmid DNA. This creates DNA fragments of various sizes and when subjected to gel electrophoresis reveals the nature of the plasmid as well as the orientation of the DNA fragment. The digestion process was carried out by incubating 3μl of the purified plasmid DNA with 0.5μl of restriction enzyme and a buffer at 37^0C for 1 hour.

The software Gene Construction kit 2 was used to simulate the gel patterns produced by digestion of the plasmids with various restriction enzymes. Figure 8.5 shows simulated gel patterns for the 10 plasmids created, when digested with various restriction enzymes. The enzymes for each plasmid were selected on the basis of the most prominent difference between the two possible orientations of insertion of the DNA fragment (PCR product) into the plasmid. Only five simulations were necessary for the 10 plasmids since the 5 corresponding to *mnm-4*(*et4*) are identical to the 5 corresponding to *sa580* (have the same *ppn-1* DNA fragment).

The digested product corresponding to 4 minipreps were subjected to gel electrophoresis and the results compared with the simulated gel pattern (Figure 8.5). This helped to identify the bacterial cultures that had taken up the right plasmid and the orientation of DNA fragment (PCR product) insertion. From the four bacterial cultures one was selected and four more minipreps prepared out of it. The resulting plasmid DNA in the four minipreps were pooled together. Another digestion with restriction enzymes and subsequent gel electrophoresis was carried out on the digested pooled plasmid DNA to verify that the right plasmid has been obtained. Figure 8.6 shows the plasmid maps with restriction sites corresponding to various restriction enzymes used.

Subsequently the concentration of the plasmid DNA was measured using a Nanodrop spectrophotometer (Thermoscientific USA). DNA molecules show strong absorption at around the optical wavelength of 260nm. The nanodrop spectrophotometer measures the optical density of a drop of DNA solution at 260nm to measure the DNA density. The higher the concentration of DNA in the solution, the higher will be the measured optical density.

8.4.7 Sequencing

The plasmids were subsequently prepared for DNA sequencing. A set of sequencing primers were designed for each of the five *ppn-1* DNA fragments. The primers were designed as per the following rules:

1. Primers should have a length of 18-20 mers.
2. The combined amount of G and C bases should be 50-60% .
3. At least two of the last three bases should be a G or C in the 3' end. This increases efficiency of priming.
4. The last base in the 3' end should not be a G or C.
5. 3'-ends of primers should not be complementary (ie. base pair), as otherwise primer dimers will be synthesised preferentially to any other product;

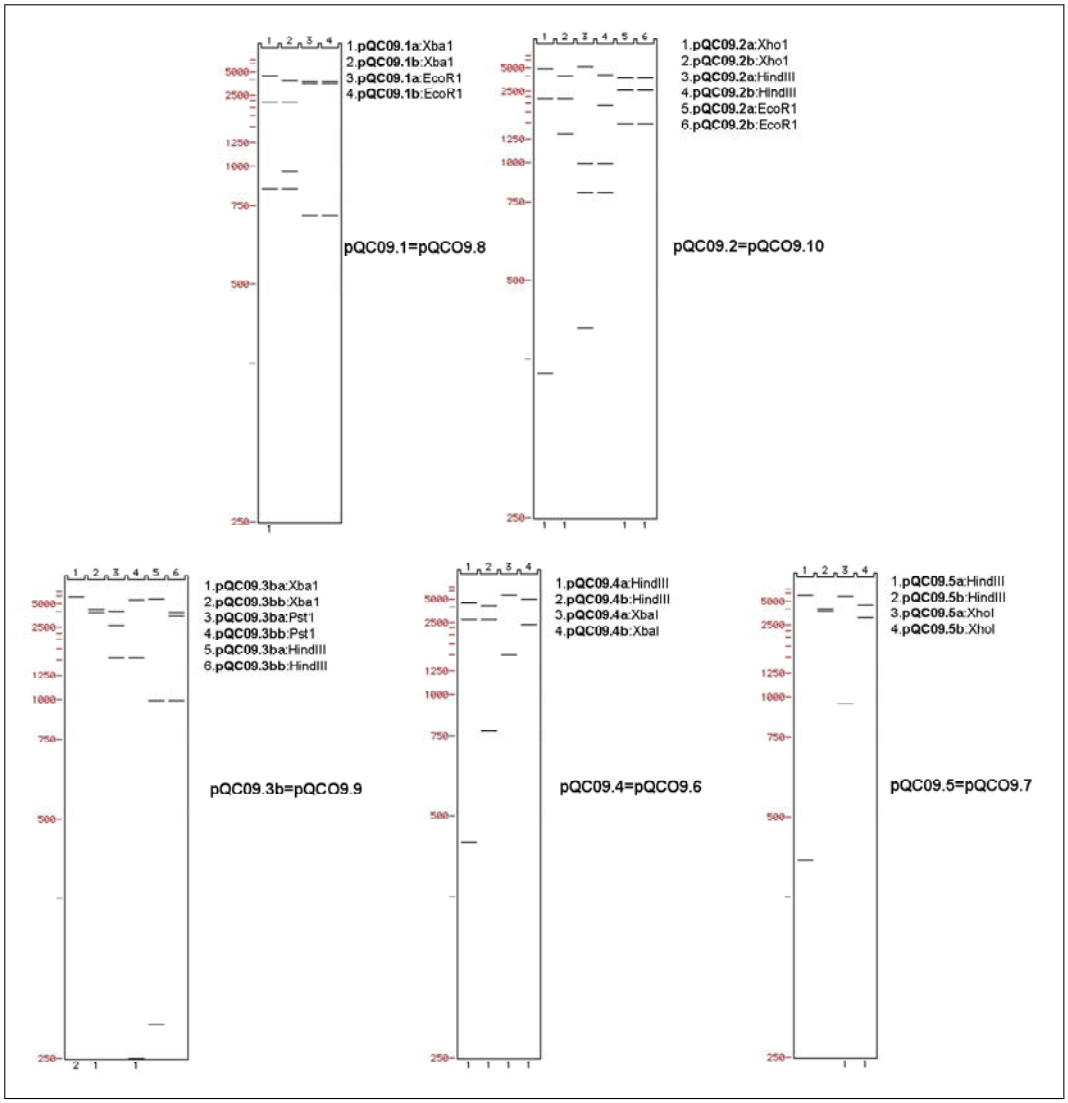

Figure 8.5: Simulated gel patterns after digestion of the plasmids with restriction enzymes

6. Avoid long stretches (more than 4) with A and T bases.

Since sequencing of a region longer than 1Kb is not very efficient, 4 -5 primers were designed for each strand of each of the five 4Kb *ppn-1* fragments. The set of primers for one strand were called the forward sequencing primers and those for the complementary strand called the reverse sequencing primers. The two sets of primers for each strand enable sequencing of each of the 4Kb *ppn-1* DNA fragment twice (in either direction). This introduces redundancy and increases robustness of sequencing result. Table 8.3 details the list of sequencing primers used. Since the sequencing was performed on the recombinant plasmid (DNA fragment of interest inserted into pCR®II Blunt Topo vector), two additional sequencing primers (M13 uni(-21) and SP6), were used that bind respectively to the two ends of the vector. This helps to sequence the very ends of the insert, which would have been difficult had the DNA fragments been sequenced without inserting them

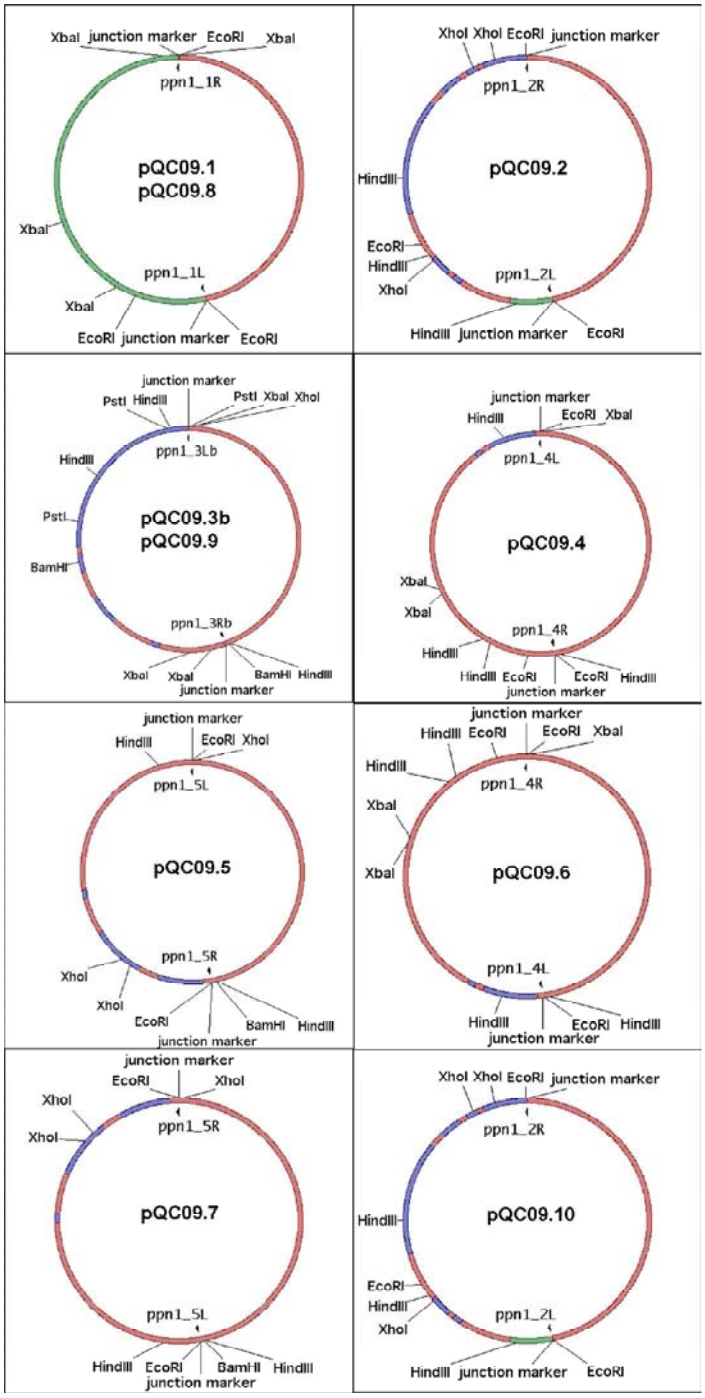

Figure 8.6: Plasmid maps with restriction sites

into a plasmid vector.

For sequencing the plasmids were diluted to the required concentration in water and shipped in separate tubes (one for each primer) to the company Eurofins MWG Operon (Germany). Sequencing results were obtained for each of the 10 plasmids and ana-

lyzed on the software 'Sequencher'. This program helped to compare the obtained sequence with the wild type *ppn-1* sequence obtained form *C.elegans* database Wormbase (www.wormbase.org). The program automatically aligns the obtained sequence of the fragment of the gene with the region in wild type gene data to which this region corresponds. The program then searches for changes in bases, in the obtained sequence with respect to the reference wild type gene sequences.

Table 8.3: List of sequencing primers

DNA Fragment	Sequencing Primer Forward	Sequencing Primer Reverse
pQC09.1 pQC09.8 ppn1_1	SEQ1_F1:5'-TTCCTCTGATCATCCGGT-3' SEQ1_F2:5'-CCTTTTCAAATCAAAGCA-3' SEQ1_F3:5'-AATGGGATGTGAGCAGGT-3' SEQ1_F4:5'-TCCAGATGACTCTTCCCA-3'	SEQ1_R1:5'-TAAGATTGATTTGACGGA-3' SEQ1_R2:5'-TGCCAATCTCATCGCGGT-3' SEQ1_R3:5'-CCTGAAAGTGAAGAACGT-3' SEQ1_R4:5'-TTGTCTCTCGTTCTAGGA-3'
pQC09.2 pQC09.10 ppn1_2	SEQ2_F1:5'-GCAGTGGCAGCAGAGAGCA-3' SEQ2_F2:5'-GACAGTGCAGGTTCGTGGAC-3' SEQ2_F3:5'-TGATGGGGAATGTCTTCCA-3' SEQ2_F4:5'-GTTGAGGATGGAAACTGCA-3' SEQ2_F5:5'-CGATACTGAGGAGACTCGT-3'	SEQ2_R1:5'-GTTCCATTCTCCAGTGACA-3' SEQ2_R2:5'-GAGAAGAGCAACGGTGAGCT-3' SEQ2_R3:5'-GCTCCAGTGCAGTCACCACT-3' SEQ2_R4:5'-ATGAAGGTATGGCTTCTGGA-3' SEQ2_R5:5'-GGAAAACGATCGAGTTCGGT-3'
pQC09.3b pQC09.9 ppn1_3	SEQ3_F1:5'-AAGCTGCGCCCAGAGCCA-3' SEQ3_F2:5'-GATTCAATCTGCTGAGCA-3' SEQ3_F3:5'-GCTTCAGCCGGAATTGGT-3' SEQ3_F4:5'-GACACGGCAATGCTGCCT-3' SEQ3_F5:5'-ATCAGATATGGAGTAGCT-3'	SEQ3_R1:5'-CAAGTGGCAAACTTGGGA-3' SEQ3_R2:5'-TTGCAGGTTCCGTCGGCT-3' SEQ3_R3:5'-GCTGAGCTCCGTGAACGA-3' SEQ3_R4:5'-GGGCAACAGTTCCTCCCA-3' SEQ3_R5:5'-GCAAGATGGCTCTCCGCA-3'
pQC09.4 pQC09.6 ppn1_4	SEQ4_F1:5'-ACTTGATCTTCTCCTTCCGA-3' SEQ4_F2:5'-TCGCCTTCAAATCCCACATC-3' SEQ4_F3:5'-GAGTCATCTCGTGATTGTGC-3' SEQ4_F4:5'-CTTACCGGTATCATCATCGT-3'	SEQ4_R1:5'-TAGACCGAATCTTACACA-3' SEQ4_R2:5'-TGGAGGAATCTATGCTGGA-3' SEQ4_R3:5'-TTACGGATCCCCAGGTACT-3' SEQ4_R4:5'-CAGTTCCACGAAAGGACACA-3'
pQC09.5 pQC09.7 ppn1_5	SEQ4_F1:5'-GTATTCTCAATTGAGAGCTG-3' SEQ4_F2:5'-CCTGTTATAAGTACAGCG-3' SEQ4_F3:5'-TAGGCTGAGGTAGGTAGGCT-3' SEQ4_F4:5'-AACTGGTCCCATGAGAGT-3'	SEQ4_R1:5'-TAACTGGCGTGGATGCAGA-3' SEQ4_R2:5"-TAGTCACCTGACTCCGCAT-3' SEQ4_R3:5"-CGCTGTACTTATAACAGGT-3' SEQ4_R4:5"-GGTGTTCACTTGCTCAGA -3'

8.4.8 Creating genetic crosses

To study genetic interaction a cross was created between the strains *mnm-4(et4)* and *sa580*. This was done by crossing *mnm-4(et4)* males with *sa580* hermaphrodites. The first step in the process was obtaining males out of *mnm-4(et4)* hermaphrodite population. In *C.elegans* males (X0) are produced by fusion of null0-X gametes (gametes that lack X chromosome) with and normal X bearing gametes. Since male sperm contains an equal frequency of null0-X bearing gametes and X-bearing gametes and since male derived sperm outcompete hermaphrodite sperm in the fertilization of oocytes, reproduction by mating produces a high number of males. In the hermaphrodite germ line null0-X gametes are produced with a very low probability by spontaneous non-disjunction of the X chromosome during meiosis in the germ line. This produces male progeny in self fertilized

hermaphrodites. The probability of spontaneous non-disjunction increases for example when the hermaphrodites are heat shocked. This fact was utilized to obtain male progeny from self fertilized hermaphrodites.

20 plates with four *mnm-4(et4)* L4 stage hermaphrodites were heat shocked at 30^0C for 6 hours and subsequently moved to 20^0C. About 20 males were obtained form the self fertilized progeny of these worms. These males were crossed with *mnm-4(et4)* hermaphrodites to produce increased numbers of *mnm-4(et4)* males. This was done by placing five *mnm-4(et4)* young males in a mating plate with three *mnm-4(et4)* L4 hermaphrodites.

The cross was setup by placing three young *mnm-4(et4)* males with one *sa580* L4 hermaphrodite in a mating plate. Around 20 mating plates were likewise prepared. Once the hermaphrodites mature and are about to lay eggs each of these hermaphrodites are picked and transferred to a fresh plate each. After 2–3 hours the eggs in each of the 20 plates are transferred to another 20 fresh plates leaving the hermaphrodites behind. 60–63 hours after the eggs were transferred, when the worms are in L4 stage half of the plates were observed to look for presence of males. Only those plates are retained that have males and the rest are discarded. Presence of males indicate that the cross had worked and the plate contained heterozygous (*mnm-4(et4);sa580*) F1 progeny. Hermaphrodites are picked form these plates and imaged. The same is done with the other half of plates 24 hours later (84–87 hours after the eggs were transferred) to look at adult heterozygous (*mnm-4(et4);sa580*) worms.

8.4.9 DIC and fluorescence imaging

For microscopic analysis, worms were mounted on 2% agarose pads, paralyzed with a small drop of anesthetic (100mM levamisole), and covered with a coverslip. These were then examined with a Zeiss Axioplan upright compound microscope using DIC optics or an FITC filter set to visualize GFP. Digital images were acquired using an attached AxioCam digital camera.

8.4.10 Scoring worms for twisted pharynges

The scoring was performed by first imaging the worms with DIC optics under 1000X magnification at a focal plane that best showed the most pronounced angle of twist in the upper half of the worm (ie starting from the coverslip side). For the transgenic worms, a photograph was first taken and subsequently the animal checked under UV illumination to check if it expressed GFP in its coelomocytes. If it did, the photograph was saved. If not it means the worm did not have the transgene and the photograph is discarded. This procedure was adopted to avoid any bias when taking the photograph: the photographer does not have apriori knowledge of whether the worm under observation has the transgene or not before taking a photograph of the pharynx. The angle of twist was measured by loading the images one by one into the image processing and analysis software Image-J (NIH, USA) and using the function provided in the software to measure angles.

8.5 Results

8.5.1 Scoring rescued transgenic lines

As part of a follow up to inconclusive previous efforts, attempts to rescue the twisted pharynx phenotype were performed by microinjection. The cosmids ZK742 and C373 were microinjected along with the marker pCC::GFP in *sa580*. The marker was used to identify the transgenic animals. The worms that have the transgene have their coelomocytes fluorescing green when observed under the epi-fluorescence microscope. A set of five transgenic lines were obtained. The rescue attempts were preformed in *sa580* rather than *mnm-4(et4)* since *sa580* is recessive while *mnm-4(et4)* is semi-dominant. These lines were named transgenic line C (Tg_C), transgenic line O (Tg_), tansgeninc line H (TG_H), transgenic line J (TG_J) and transgenic line P (Tg_P). As part of the work described in this chapter, these transgenic lines along with *mnm-4(et4)*, *sa580*, and N2 were scored for their twist in the pharynx.

The scoring was performed as described in section 8.4.10. The results are shown in table 8.4. The table shows the number of worms imaged, the average angle of twist, the standard deviation in the measured angles, and the standard error of mean. As seen from the table the cosmids ZK742 and C373 were able to produce a sizable number of rescues in three transgenic lines created namely Tg_H, Tg_J and Tg_P. Figure 8.7 shows the pharynx of A) a wild type N2 worm which does not have the twisted pharynx phenotype, B) a *sa580* worm which has a twisted pharynx (degree of twist indicated in the figure) and C) a *sa580* worm that has been rescued using cosmids ZK742 and C373 . In the rescued worm it can easily be appreciated that the pharynx shows a wild type phenotype. These results further confirmed the possibility that the mutation lies within the gene *ppn-1* since the cosmid ZK742 has the promoter for this gene and C373 the coding region.

Table 8.4: Measurement of degree of twist in N2, *sa580* and various transgenic lines attempted to rescue SA580 twisted pharynx phenotype

	N2	SA580	Tg_C	Tg_O	Tg_H	Tg_J	Tg_P
Number	10	24	17	11	25	27	11
Average (degrees)	2.32	13.7	12.62	12.2	7.86	5.3	8.7
Standard Deviation	1.09	2.32	4.118	4.24	3.08	3.2	6.47
Standard Error of Mean	0.345	0.473	0.998	1.278	0.616	0.615	6 1.95

8.5.2 Sequencing results

By sequencing the *ppn-1* gene in the strains *mnm-4(et4)* and *sa580* it was confirmed that the mutation was indeed in this gene and the location of the mutation in each of these strains were determined. The results are shown in the Table 8.5. The table shows the *ppn-1* fragment in which the mutation was found, the recombinant plasmid that had the fragment as an insert, the location of mutation in terms of the number of the amino acid, the change in amino acid as a result of this mutation and finally the mutation names.

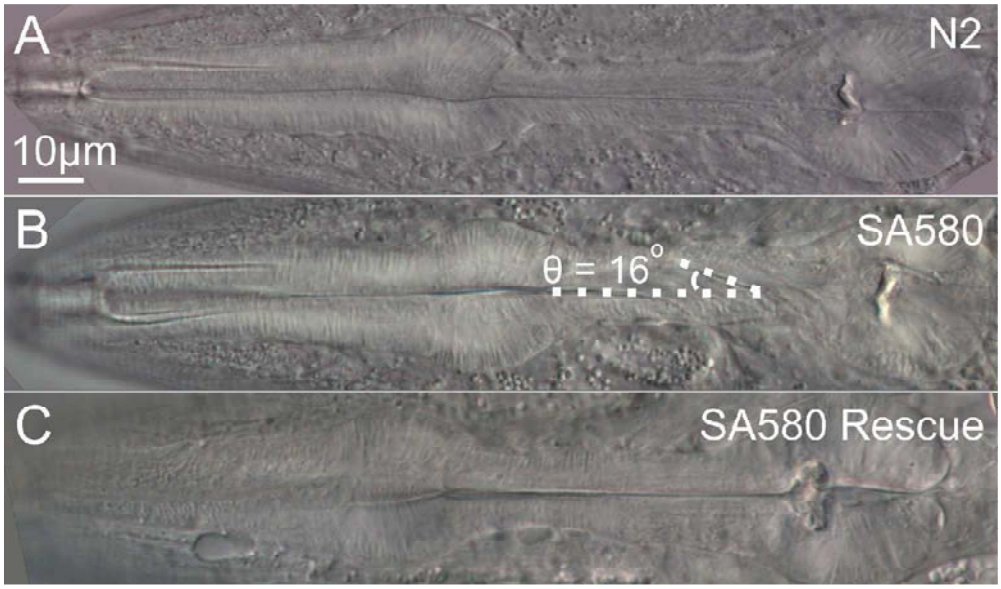

Figure 8.7: *C.elegans* pharynges A) N2 wild type, B) *sa580* which has a twisted pharynx (degree of twist θ , indicated in the figure), C) *sa580* with twisted pharynx phenotype rescued.

Once the results were obtained the plasmids pQC09.3bb and pQC09.9b were created again starting from the PCR amplification of the ppn1_3 and sequenced again. This repetition was done to rule out any PCR artifact producing the mutations rather than a mutation in the strain. The repeated set of experiments confirmed the mutations.

Table 8.5: Details of the mutation found in *mnm-4(et4)* and *sa580*

Strain	*ppn-1* fragment	Plasmid	Location of Mutation in the gene	Amino Acid Change	Mutation Name
sa580	ppn1_3	pQC09.3b	965	Glycine to Glutamic Acid	G965E
mnm-4(et4)	ppn1_3	pQC09.9b	973	Cysteine to Tyrosine	C973Y

The following facts about the mutations can be noted:

- Both *sa580* and *mnm-4(et4)* have the mutation in the gene *ppn-1*.
- Since both these strains have the mutation in the same gene it is confirmed that *sa580* and *mnm-4(et4)* are alleles of each other.
- Both mutations caused a G⟶ A (Guanine to Cytosine) transition. This is very common in EMS (Ethylmethane Sulphonate) induced mutations, which was used to induce these mutations.

- The location of mutation in *sa580* as well as *mnm-4(et4)* are very close to each other (only 24 base pairs apart) and they affect the same region in the protein (*C.elegans* papilin).

8.5.3 Genetic interaction between *mnm-4(et4)* and *sa580*

To check the genetic interaction between *mnm-4(et4)* and *sa580*, these strains were crossed as described in section 8.4.8 to obtain the heterozygous strain *mnm-4(et4);sa580*. The twist in the pharynx was observed in the crossed strain and compared to the parental strains. The results are shown in table 8.6 . The table shows the number of worms imaged, the average degree of twist, the standard deviation in the degree of twist and the standard error of mean. In each set *mnm-4(et4);sa580*, *mnm-4(et4)* and *sa580*) the imaging was performed at two life stages L4 (60–63 hours after picking the embryos) and Adult (84–87 hours after picking the embryos). Figure 8.8 shows images of *C.elegans* pharynges of the crossed and parental strains in the L4 stage. Figure 8.9 shows the *C.elegans* pharynges of the crossed and parental strains in adult stage.

Table 8.6: Measurement of degree of twist in *mnm-4(et4);sa580*, *mnm-4(et4)* and *sa580*

	mnm-4(et4); sa580 (L4)	*mnm-4(et4); sa580* (Adult)	*mnm-4 (et4)* (L4)	*mnm-4 (et4)* (Adult)	*sa580* (L4)	*sa580* (Adult)
Number	20	31	25	34	39	30
Average (degrees)	10.47	13.126	10.3	13.35	9.68	13.39
Standard Deviation	0.756	1.836	1.719	1.664	0.994	1.225
Standard Error of Mean	0.169	0.33	0.343	0.285	0.159	0.223

It is clear form the above measurements and figures that the genetic cross between *mnm-4(et4)* and *sa580* shows the same parental phenotype. The degree of twist in the heterozygous is very similar to the degree of twist in the parental strains.

8.5.4 Twist in the amphid neurons

The twist in the pharynx of the *sa580* strain was initially observed by noting the twist in the amphid neurons. *C.elegans* has 11 pairs of bilaterally symmetric chemosensory amphid neurons. They have their cell bodies outside the nerve ring and have cliated dendrites. The dendrites are bundled and pass parallel to the longitudinal axis of the pharynx on either side of the pharynx and pass on to the nose. Even though the dendrites donot pass through the pharynx, they pass very close to it. The cilia at the tip of the dendrite are exposed to the outside environment that helps them in their chemosensory function. This exposure to the outside environment also helps staining a number of these amphid neurons by simply incubating the worms at room temperature in a dye such as DiI. The neurons take up the dye through their exposed ends and can be subsequently observed under UV light using a red filter.

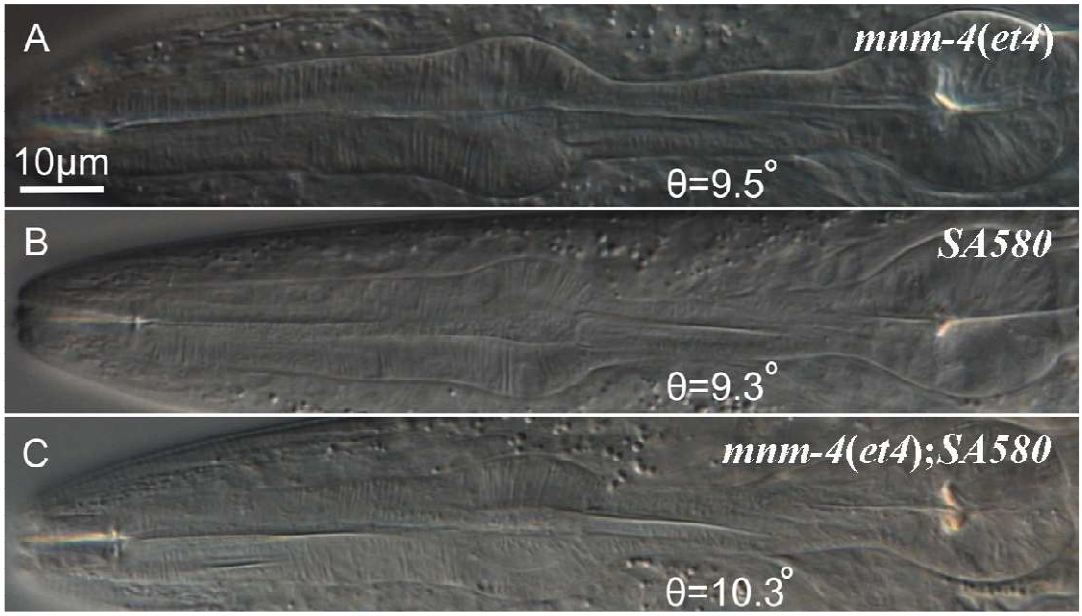

Figure 8.8: *C.elegans* pharynges in L4 larval stage A) *mnm-4(et4)*, B) *sa580*, C) *mnm-4(et4);sa580*. The degree of twist θ is indicated in the figure for each case.

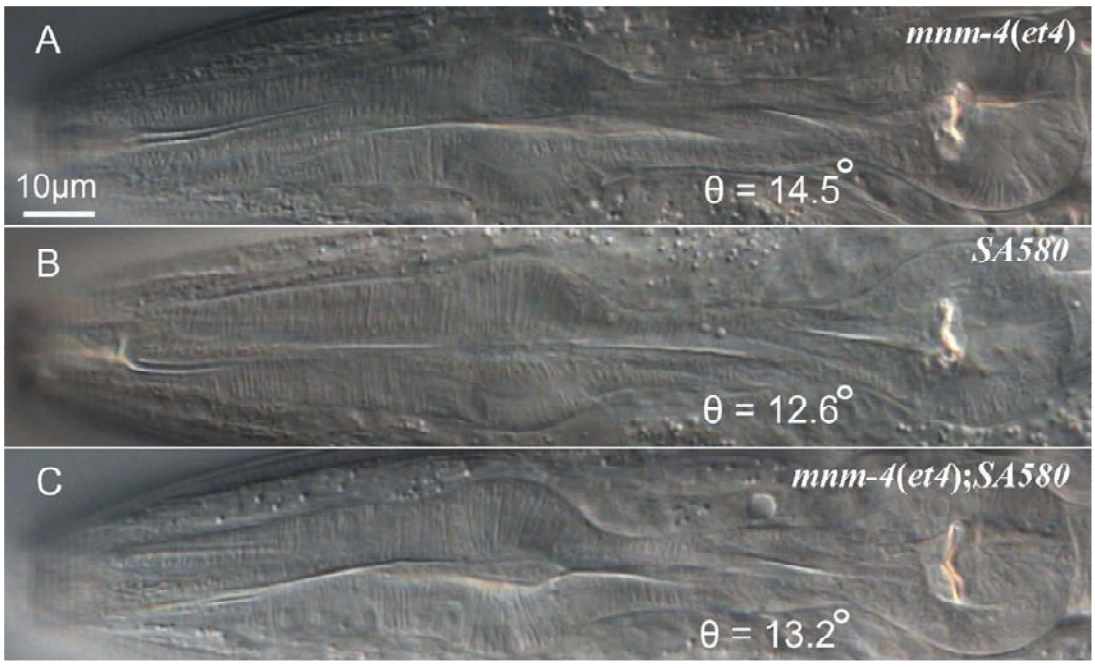

Figure 8.9: *C.elegans* pharynges in Adult stage A) *mnm-4(et4)*, B) *sa580*, C) *mnm-4(et4);sa580*. The degree of twist θ is indicated in the figure for each case.

The amphid neurons in young adult worms in the two mutant strains and wild type N2 strains were imaged to observe the twist in the apmphid neurons. The result is shown in table 8.7. The table shows the number of worms imaged, the number of worms that had twisted pharynges and the number of worms that had twisted amphid neurons. It can be observed that it is not always that a twist in the pharynx is accompanied by a twist in the amphid neurons. Figure 8.10 shows the images of amphid neurons in the strains N2, *sa580* and *mnm-4(et4)*. The figures are a superposition of DIC image of the pharynx and the fluorescence image of the amphid neurons. For *sa580* and *mnm-4(et4)* two cases are shown, one in which the amphid neurons are twisted and another in which the amphid neurons are not twisted.

Table 8.7: Twist in amphid neurons

	N2	*mnm-4(et4)*	*sa580*
Number	20	21	20
Twisted Pharynges	0	21	20
Twisted Amphid Neurons	0	7	5

Since these dendrites donot directly pass through the pharynx it is very likely that the twist in them occur only when the bundle of dendrites get stuck onto the pharynx during development and the pharynx drags these dendrite bundles along while its twist is progressing.

8.6 Discussion

This work has primarily demonstrated that the twisted pharynx phenotype in the strains *mnm-4(et4)* and *sa580* is due to mutation in the *ppn-1* gene and that these two strains are alleles of each other.

8.6.1 Papilin Protein

The *ppn-1* gene in *C.elegans* codes for the *C.elegans* papilin protein that is homologue to the Drosophila papilin protein [235]. Papilins are a class of secreted extracelluar matrix glycoproteins that are conserved in Drosophila, *C. elegans*, mice, and humans [235]. Drosophila papilin is primarily a large glycoprotein with O-linked sulfated glycosamine chains and is major component of the basement membrane [235]. The N-terminal part of the protein is formed by a set of thrombospondin type 1 domains (TSR) separated by a specific, cysteine-rich spacer region, which, together, is named the "papilin cassette" [235]. The central region of the protein has about 500 amino acid-long sequence extremely enriched in Ser and Thr, containing many potential O-glycosylation sites [235]. The C-terminal portion of papilin includes several Kunitz-type domains and a WAP-type four-disulfide core domain. This region is homologous to known serine protease inhibitors [236]. The papilin cassette of papilin is homologous with the noncatalytic portion of the ADAMTS family of secreted metalloprotease. Papilin binds to ADAMTS family of proteases and possibly inhibits them and plays a role in localizing the action of these pro-

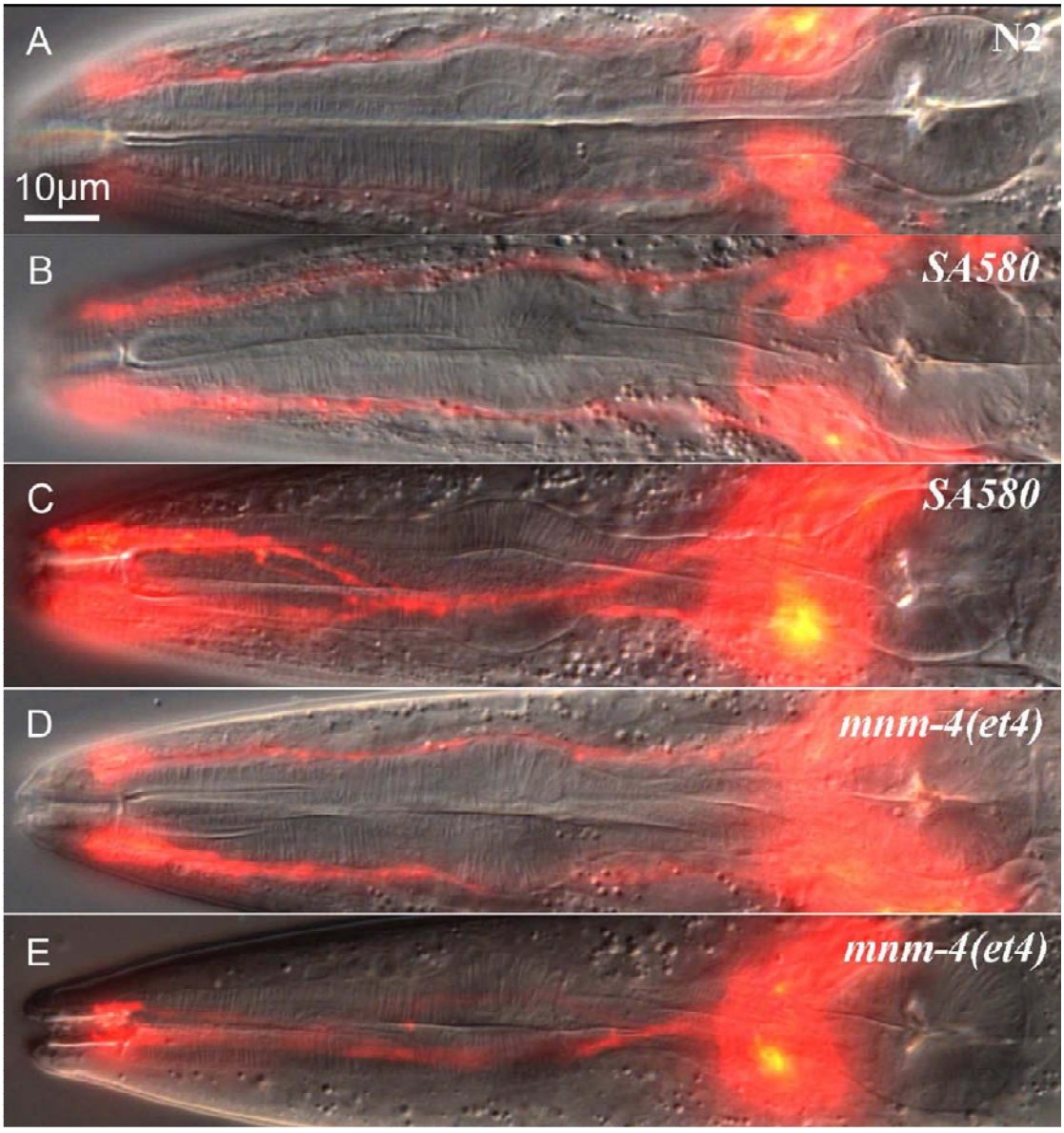

Figure 8.10: Superposition of DIC image of the pharynx and the epi-fluorescence image of amphid neurons A) N2 B) *sa580* with normal amphid dendrites C) *sa580* with twisted amphid dendrites, D) *mnm-4(et4)* with normal amphid dendrites E) *mnm-4(et4)* with twisted amphid dendrites

teases [235]. In drosophila 3 splice variants of the protein exist which are named Papilin-1, Papilin-2 and Papilin-3. They differ in the number of Kunitz domains and IgC2 domains in the C terminal [236]. Papilin-1 is the shortest and Papilin-3 is the longest. Papilin-1 is expressed during early embryo development and apparently plays role in localizing the action of ADAMTS family of proteases. Papilin-2 is most abundant papilin protein in drosophila and forms a major component of the basement membrane. Papilin-3 forms a component of the protective lining in the embryonic dorsal vessel and in the peritrophic

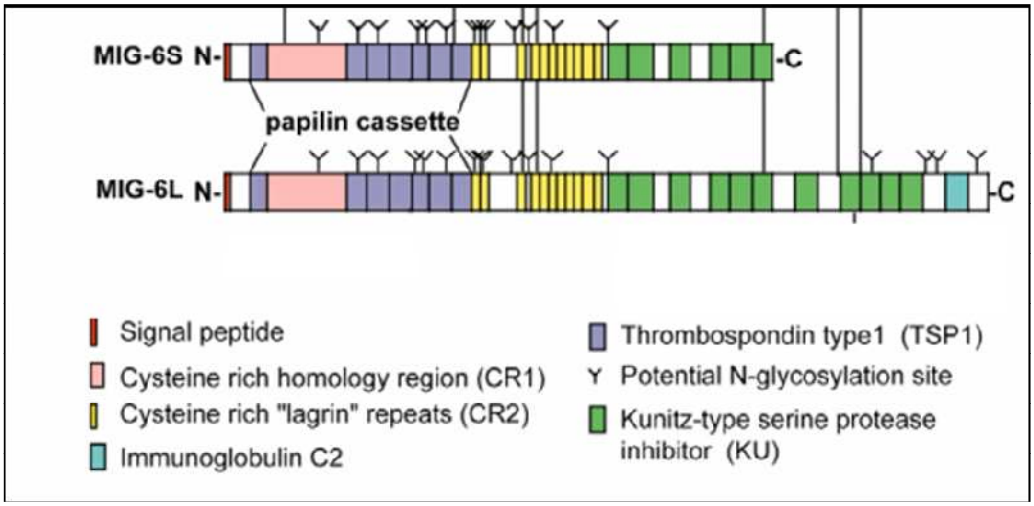

Figure 8.11: Protein domain structure of MIG-6S and MIG-6L (adapted from ref.[237])

membrane of the gut [236].

A recent work has described more functions of the *C.elegans* papilin protein [237]. As a result of this work the *ppn-1* that codes for *C.elegans* gene has been renamed *mig-6*. Two classes of mutations in the *mig-6* gene were identified: Class-l which shows an extremely slow DTC (Distal Tip Cell) migration compared to the wild type and results in foreshortened gonad arms and Class-s in which the DTCs migrate at an approximately normal rate but have specific defects in phase 2 migrations [237]. Two mRNAs encoded by *mig-6* were discovered and designated *mig-6S* and *mig-6L*. *mig-6S* translates a protein (MIG-6S) with 11 exons and *mig-6L* translates a protein (MIG-6L) with whole of the 10 exons as in *mig-6S* a part of exon 11 and a 12th exon [237]. *mig-6L* alone normally encodes class-l functions that are required post-embryonically for a wild-type rate of DTC migration [237]. *mig-6S* is apparently required in embryogenesis and its lack leads to early embryonic and larval lethality. Loss of *mig-6S* post embryonically phenocopies the phase 2 DTC defects seen in class-s mutants [237]. The protein domain structures of MIG-6S and MIG-6L are shown in Figure 8.11 [237].

mig-6(s) mutations affect distribution of the MIG-17 metalloproteinase [237]. This substantiates the argument that the papilin protein acts to localize the function of metalloproteinases [235]. A reduction in collagen IV protein or a reduction in collagen IV folding and secretion (caused by point mutation) was shown to suppress *mig-6* class-s DTC defects. These results indicate that collagen IV acts antagonistically to MIG-6S in an extracellular mechanism that affects phase 2 DTC migration [237].

8.6.2 Allometric growth model of pharyngeal twist

Both of the mutations in *mig-6* gene that causes the pharyngeal twist (*mnm-4(et4)* and *sa580*) cause defects in the CR2 region (see Figure 8.11) of the *C.elegans* paplilin protein and likely affect both the isoforms of the protein MIG-6S and MIG-6L. It is however unclear as of now how this causes a pharyngeal twist. The pharynx consists of number of cells including 34 muscle cells that have different sizes and shapes. Hence it is

important that these cells grow at different rates (allometric growth), while they develop, so as to account for the different sizes but still grow together. During this process the cells have to attach and reattach to the extracelluar matrix. The metalloproteinases apparently aid in this process by loosening the stiff extracelluar matrix components like collagen and creating attachment points. Also these proteases could help create the extra space required to accommodate the growth of the pharynx.

Since one of the functions of the papilin protein is to localize the function of these metalloproteinases, it is very likely that in mutants of *mig-6* gene this function is not properly carried out. This could cause abnormal allometric growth. Some regions of the extracelluar matrix may not loosen enough resulting in some sort of opposition to the growth that could result in a torque that eventually results in a twisted pharynx.

In addition the signals form the extracelluar matrix that directs the growth of cytoskeletal components could get perturbed in a mutant with papilin defects resulting in some of these components growing longer than usual and that could result in the pharynx getting twisted to accommodate the longer cytoskeletal components.

Chapter 9

Conclusion and Future Prospects

9.1 Conclusions

The research described in this thesis has primarily looked at use of light as a tool to guide the axons of neurons *in-vitro* as well as to use it to induce submicrometer incisions in axons of neurons *in-vivo* in the model organism *C.elegans*.

Our initial investigations revealed that NIR femtosecond light spot of very low average power when placed at a small distance form the growth cones of primary neuronal cell cultures are able to significantly change the orientation of filopodia towards the light spot. This was however not observed when CW light was used in the same condition with the same average power. This indicated the ability of femtosecond light to induce some sort of signaling effect on the growth cone of primary neuronal cell cultures.

Since filopodia are the fundamental sensors in the growth cone that direct axonal growth, an orientation of filopodia in a particular direction indicates preferred axonal growth in that direction. To investigate if the initial response of filopodia to distantly placed femtosecond light sources could manifest on the whole axon, experiments were repeated for longer durations of time. It was observed that in a significant number of cases the initial orientation of the filopodia towards distantly placed femtosecond laser light manifests onto the growth of the whole axon towards these light sources.

Now it was not clear if it was the high intensity of the femtosecond light that was responsible for the effect or the pulsed nature of femtosecond light (no related to the high peak intensity) that was causing this effect. Further investigation using chopped NIR CW light (same average power) which would impart a pulsed character to the light spot without a high peak intensity, revealed that the response of the axons were exactly similar to the use the femtosecond light. The percentage of attracted axons were almost the same when chopped CW light was used as when femtosecond light was used. Hence it seems that growth cones can respond to the presence of distantly placed NIR pulsed laser sources.

The question that needs to be answered is to why such an effect should take place. At this moment there are no definite answers to this question. An interesting hypothesis is that cells in general communicate among themselves using modulated NIR light. The modulation apparently helps them distinguish the weak signals from background noise. When an external source of light is placed, a cross talk could be generated. Or in other words the neurons could be to mistaking the distantly placed light sources to be other

neurons and they could be growing axons towards these in a bid to form networks.

The next logical thing to be done was to explore similar effects *in-vivo*. This however put forward a technical hurdle. We lacked a tool that could induce optical stimulation and at the same time image the results of stimulation live using a multitude imaging modalities. It was principally with this in mind that we went on to develop mutimodal optical workstation. The workstation extends a commercially available confocal microscope (Nikon Confocal C1-Si) to include nonlinear/multiphoton microscopy and optical manipulation/stimulation tools such as nanosurgery.

The setup allows both subsystems (confocal and nonlinear) to work independently and simultaneously. The workstation enables, for instance, nanosurgery along with simultaneous confocal and brightfield imaging. The nonlinear microscopy capabilities are added around the commercial confocal microscope by exploiting all the flexibility offered by this microscope and without need for any mechanical or electronic modification of the confocal microscope systems. As an example, the standard differential interference contrast condenser and diascopic detector in the confocal microscope are readily used as a forward detection mount for second harmonic generation imaging.

For the control and automation of the various experiments that were intended to be performed with the multimodal workstation a number of virtual automation and control programs were written in the virtual instrumentation Labview and used extensively in the research described in this thesis.

One of first applications of the multimodal optical workstation was its use in performing Nano-neurosurgery and observing the dynamics associated with the process by multimodal imaging of the procedure live using a multitude of imaging modalities. A number of effects like spilling of axoplasm, laser induced muscular contraction etc: were observed. A through assessment of collateral damage could also be performed. The ability of the multimodal system to assess collateral damage is much superior to the currently established ways of detecting collateral damage after Nano-neurosurgey. In addition Second Harmonic Generation (SHG) microscopy was introduced as a novel technique to detect collateral damage to the muscle surrounding the neurite targeted for Nano-neurosurgery.

A better understanding of the phenomenon like axon guidance and neuron regeneration after Nano-neurosurgery requires a deeper understanding of biology especially molecular biology and genetics. With the motive of having a better understanding of these fields, some time was spent in a molecular biology and genetics lab in Gothenburg, Sweden. Investigation was basically performed to determine the mutations responsible for inducing a twist in certain neuronal processes in two strains of *C.elegans*. Using a set of molecular biology methods both the mutations were located in the *mig-6* gene. The mutation causes a defect in the extracellular matrix protein *C.elegans* papilin.

9.2 Future Prospects

The work on guiding neurons with light offers many possibilities for future research. The mechanisms leading to this effect need to be discovered. For this dynamics of actin and calcium for example can be studied by staining the neurons using fluorescent markers and imaging using epi-fluorescence or confocal microscopy while the pulsed NIR beam spot is used to guide the axon. The multimodal optical workstation is ideally suited (provides ability for NIR stimulation and simultaneous imaging) for these studies. Actin is the

most important cytoskeletal element and calcium is a very important second messenger in the process of neuron guidance. Hence studying dynamics of these could give significant clues about the mechanisms behind optical signaling of growth cones. In addition opsin-3, which is the family of putative light sensors in the deep brain neurons can be investigated. The expression of various opsins in the cortical neurons and their response to pulsed NIR should also help a great deal to understand the mechanism.

Discovery of the most optimum recipe that provides the most efficient response form the growth cones signaled using NIR pulsed light still needs further efforts. The parameters like optical power, wavelength, operation regime, culture media, type of neurons etc: can be varied and investigated for the most efficient response. The effect also needs to be investigated *in-vivo* in model organisms like *C.elegans* and higher order organisms like mouse. Such studies could also involve of the use of electro-physiological or optical techniques to investigate the electrical activity of neurons subjected to optical signaling.

There are a lot of improvements that are possible to the multimodal optical workstation. Aberration correction optics, beam shaping optics and dispersion compensation optics could be added to the current system to achieve non-linear effects with minimum usage of optical energy. A regenerative amplifier could be added and Nano-neurosurgery performed using amplified femtosecond laser pulses that would impart tighter control over the surgical process and minimize collateral damage. THG can replace SHG if longer wavelengths for excitation are used. It is also possible to image THG and SHG simultaneously by adding another dichoric mirror in a fourth filter cube (FC4) that could be placed above the filter cube FC3 (positioned on top of the condenser). If a dichroic is so selected, so as to reflect the THG, it could be detected by a detector placed outside the microscope while the SHG could be allowed to propagate into the optical fiber in the diascopic detector.

The control software for the confocal and multiphoton subsystems could be integrated into one, to achieve better synchrony between the two subsystems. The nonlinear component of the system can also be used to induce linear effects, like optical tweezing, merely by switching the laser mode to CW. For example, while the second system performs optical tweezing, the confocal or epi-fluorescence component could be imaging the procedure in real time.

Many biological problems related to fundamental neuroscience can be approached by the Nano-neurosurgery tool. Severing of axons can be used to better understand neuronal function and development. Nano-neurosurgery can also be attempted on higher order organisms like mouse by making cranial optical windows. Neuron regeneration after surgery can be investigated in various *C.elegans* mutants to discover novel mechanisms of nerve regeneration.

The many discovered dynamic effects like muscular contraction, and spreading of autofluorescence due to muscular stimulation can be further investigated. The multimodal optical workstation can be used for femtosecond laser stimulation of muscle which can open up many interesting avenues of study, especially in *C.elegans*. Many other effects related to muscular simulation can be investigated. The aperture and closure of cuticle as a result of the induced cavitation bubble during neurosurgery could be used to study elastic properties of the cuticle. Collateral muscle damage can be better quantified using the SHG microscopy tool and its effect on nerve regeneration studied. Such studies would throw more light on the influence of the extracellular matrix and other surrounding cells

on neuron guidance and nerve regeneration.

The nanosurgery tool can be used on other organisms like *Drosophila melanogaster*, Zebra Fish and also individual cells, tissue slices etc:. In addition to neurons the nanosurgery tool can be used to knock out of organelles like mitochondria in single cells, incise actin filaments, muscular fibrils, etc:. This can also be a very useful tool in developmental biology where individual cells in embryos could be knocked out and embryo development studied in absence of these cells. Such studies could give many insights into roles of specific cells in embryogenesis and their interaction with other cells. Photoporation is another interesting direction in which the nanosurgery tool can take us. Small pores can be drilled in individual cells and many mechanisms like exocytosis and endocytosis studied.

Bibliography

[1] S. Inoué and K. R. Spring. *Video Microscopy: The Fundamentals. 2e.* Plenum Press, New York, 1997.

[2] S. Inoué and R. Oldenbourg. *Handbook of Optics, Vol. II. 2e.* McGraw-Hill, New York, 1995.

[3] M. Abramowitz. *Contrast Methods in Microscopy: Transmitted Light.* Olympus America, Inc., New York, 1987.

[4] H. G. Kapitza. *Microscopy From The Very Beginning.* Carl Zeiss, Oberkochen, Germany, 1994.

[5] J. G. Delly. *Photography Through The Microscope. 9e.* Eastman Kodak Co., New York, 1988.

[6] G. Nomarski. *J. Phys. Radium*, 16:79S–11S, 1955.

[7] Rafael Yuste, Frederick Lanni, and Arthur Konnerth. *Imaging Neurons: A Laboratory Manual.* Cold Spring Harbor Laboratory Press, USA, 1999.

[8] M. Abramowitz. *Fluorescence Microscopy: The Essentials.* Olympus America, Inc., New York, 1993.

[9] B. Herman. *Fluorescence Microscopy. 2ed.* BIOS Scientific Publishers Ltd., Oxford, UK, 1998.

[10] F. W. D. Rost. *Fluorescence Microscopy (2 volumes).* Cambridge University Press, New York,USA, 1992.

[11] Nicholas J. Turro. *Modern Molecular Photochemistry.* The Benjamin/Cummings Pub . Co., San Francisco, 1978.

[12] Eugene A. Permyakov. *Luminescent Spectroscopy of Proteins.* CRC press, USA, 1992.

[13] T. Wilson. Optical sectioning in confocal fluorescence microscopes. *Scanning*, 154:143–156, 1989.

[14] James B. Pawley. *Handbook of Biological Confocal Microscopy. 2ed.* Springer, New York,USA, 1995.

[15] John K. Stevens, Linda R. Mills, and Judy E. Trogadis. *Three-dimensional Confocal Microscopy: Volume Investigation of Biological Specimens.* Academic Press, USA, 1994.

[16] Min Gu. *Principles of Three Dimensional Imaging in Confocal Microscopes.* World Scientific, Singapore, 1996.

[17] Alan R. Hibbs. *Confocal Microscopy for Biologists.* Kluwer Academic/Plenum Publishers, Netherlands, 2004.

[18] Barry R. Masters. *Confocal Microscopy And Multiphoton Excitation Microscopy: The Genesis of Live Cell Imaging.* SPIE Press, USA, 2006.

[19] Stephen W. Paddock. *Confocal Microscopy: Methods and Protocols.* Humana Press, New Jersey ,USA, 1998.

[20] P.C. Cheng. *Focus on Multidimensional Microscopy.* World Scientific, Singapore, 2000.

[21] M. Minsky, 1961. Microscopy Apparatus U.S Patent No. 3013467.

[22] M. Minsky. Memoir on inventing the confocal scanning microscopy. *Scanning*, 10:128–138, 1988.

[23] J. W. Lichtmann. Confocal microscopy. *Scientific American*, pages 40–45, August 1994.

[24] J. G. White, W. B. Amos, and M. Fordham. Confocal versus conventional imaging of biological structures by fluorescence light microscopy. *J. Cell Biol.*, 105:41–48, 1987.

[25] J. R. Swedlow, K. Hu, P. D. Andrews, D. S. Roos, and J. M. Murray. Measuring tubulin content in toxoplasma gondii: A comparison of laser-scanning confocal and wide-field fluorescence microscopy. *Proc. Natl. Acad. Sci. USA*, 99:2014–2019, 2002.

[26] T. Wilson and C. Sheppard. *Theory and Practice of Scanning Optical Microscopy.* Academic Press, London, 1984.

[27] T. Wilson. *Confocal Microscopy.* Academic Press, London, 1990.

[28] D. B. Murphy. *Fundamentals of Light Microscopy and Electronic Imaging.* Wiley-Liss, New York, USA, 2001.

[29] R. H. Webb. Confocal optical microscopy. *Rep. Prog. Phys.*, 59:427–471, 1996.

[30] Robert W. Boyd. *Nonlinear Optics 2ed.* Academic Press, USA, 2003.

[31] Jerome V. Moloney and Alan C. Newell. *Nonlinear Optics.* Westview Press, USA, 2003.

[32] N. Bloembergen. *Nonlinear Optics.* World Scientific, Singapore, 1996.

[33] E. G. Sauter. *Nonlinear Optics.* Wiley, USA, 1996.

[34] Richard L. Sutherland, Daniel G. McLean, and Sean Kirkpatrick. *Handbook of Nonlinear Optics.* CRC Press, USA, 2003.

[35] Y. R. Shen. *The Principles of Nonlinear Optics.* J. Wiley, USA, 1984.

[36] Kuang sheng Ho, Guang S. He, and Song H. Liu. *Physics of Nonlinear Optics.* World Scientific, Singapore, 2000.

[37] Germain Chartier. *Introduction to Optics.* Springer, USA, 2005.

[38] Barry R. Masters and Peter T.C. So. *Handbook of Biomedical Nonlinear Optical Microscopy.* Oxford University Press, USA, 2008.

[39] Peter Török and Fu-Jen Kao. *Optical Imaging and Microscopy:Techniques and Advanced Systems.* Springer, USA, 2007.

[40] Chunhui Xu. *Multiphoton Excitation of Molecular Fluorophores in Nonlinear Laser Scanning Microscopy.* Cornell University, USA, 1996.

[41] Guy Cox. *Optical Imaging Techniques in Cell Biology.* CRC Press, USA, 2007.

[42] Tuan Vo-Dinh. *Biomedical Photonics Handbook.* CRC Press, USA, 2003.

[43] Society of Photo-optical Instrumentation Engineers and Bio-Rad Laboratories. *Multiphoton Microscopy in the Biomedical Sciences.* SPIE, USA, 2005.

[44] Alan Conrad Bovik. *Handbook of Image and Video Processing.* Academic Press, London, 2005.

[45] W. Denk, J. H. Strickler, and W. W. Webb. Two-photon laser scanning fluorescence microscopy. *Science*, 248:73–76, 1990.

[46] W. Denk, J. H. Strickler, and W. W. Webb, 1991. Two-photon laser microscopy. United States Patent 5,034,613.

[47] M. Göppert. Über die wahrscheinlichkeit des zusamenswirkens zweier lichtquanten in einem elementarakt. *Die Naturwissenschaften*, 17:932, 1929.

[48] M. Göppert. Über elementarakte mit zwei quantensprüngen. *Ann. Phys. (Leipzig)*, 9:273–294, 1931.

[49] Paul. J. Compagnola and Leslie M. Loew. Second harmonic generation imaging microscopy for visualizing biomolecular arrays in cells, tissues and organisms. *Nature Biotechnology*, 21:1356–1360, 2003.

[50] Guy Cox, Eleanor Kable, Allan Jones, Ian Fraser, Frank Manconi, and Mark D. Gorrell. 3-dimensional imaging of collagen using second harmonic generation. *Journal of Structural Biology*, 141:53–62, 2003.

[51] Rebecca M. Williams, Warren R. Zipfel, and Watt W. Webb. Interpreting second-harmonic generation images of collagen i fibrils. *Journal of Structural Biology*, 88:1377–1386, 2005.

[52] D. A. Dombeck, K. A. Kasischke, H. D. Vishwasrao, M. Ingelsson, B. T. Hyman, and W. W. Webb. Uniniform polarity microtubule assemblies imaged in native brain tissue by second-harmonic generation microscopy. *Proceedings of the National Academy of Sciences. USA*, 100:7081–7086, 2003.

[53] Andrew C. Millard Sergey V. Plotnikov and, Paul J. Campagnola, and William A. Mohler. Characterization of the myosin-based source for second-harmonic generation from muscle sarcomeres. *Biophysical Journal*, 90:693–703, 2006.

[54] William Mohler, Andrew C. Millard, and Paul J. Campagnola. Second harmonic generation imaging of endogenous structural proteins. *Methods*, 29:97–109, 2003.

[55] Martin Both, Martin Vogel, Oliver Friedrich, Frederich von Wegner, Thomas Knsting, Rainer H. A. Fink, and Dietmar Uttenweiler. Second harmonic imaging of intrinsic signals in muscle fibers in situ. *Journal of Biomedical Optics*, 9:882, 2004.

[56] Guy Cox, Nuno Moreno, and José Feij´o. Second-harmonic imaging of plant polysaccharides. *Journal of Biomedical Optics*, 10:024013, 2005.

[57] R. Malcom Brown Jr., Andrew C. Millard, and Paul J. Campagnola. Macromolecular structure of cellulose studied by second-harmonic generation imaging microscopy. *Journal of Biomedical Optics*, 28:2207–2209, 2003.

[58] Simin Feng and Herbert G. Winful. Physical origin of the gouy phase shift. *Opt. Lett.*, 26:485–487, 2001.

[59] Y. Barad, H. Eisenberg, M. Horowitz, , and Y. Silberberg. Nonlinear scanning laser microscopy by third harmonic generation. *Appl. Phys. Lett.*, 70:922–924, 1997.

[60] A. Squier, M Muller, G. J. Brakenhoff, and K. R. Wilson. Third harmonic generation microscopy. *Opt. Exp.*, 3:315–324, 1998.

[61] D. Yelin and Y. Silberberg. Laser scanning third-harmonic-generation microscopy in biology. *Opt. Exp.*, 5:169–175, 1999.

[62] Andrew C. Millard, Paul W. Wiseman, David N. Fittinghoff, Kent R. Wilson Jeffrey A. Squier, and Michiel Muller. Third-harmonic generation microscopy by use of a compact, femtosecond fiber laser source. *Appl. Opt.*, 38:7393–7397, 1999.

[63] L. Canioni, S. Rivet, L. Sarger, R. Barille, Pierre Vacher, and Pierre Voisin. Imaging of ca2+ intracellular dynamics with a third-harmonic generation microscope. *Opt. Lett.*, 26:515–517, 2001.

[64] Shi-Wei Chu, Szu-Yu Chen, Tsung-Han Tsai, Tzu-Ming Liu, Cheng-Yung Lin, Huai-Jen Tsai, and Chi-Kuang Sun. In-vivo developmental biology study using noninvasive multi-harmonic generation microscopy. *Opt. Exp.*, 11:3093–3099, 2003.

[65] Dan Oron, Dvir Yelin, Eran Tal, Sefi Raz, Rachel Fachima, and Yaron Silberberga. Depth-resolved structural imaging by third-harmonic generation microscopy. *J. Struct. Biol.*, 147:3–11, 2004.

[66] D. Debarre, W. Supatto, A.M. Pena, A Fabre, T. Tordjmann, L Combettes, M.C. Schanne-Klein, and E. Beaurepaire E. Imaging lipid bodies in cells and tissues using third-harmonic generation microscopy. *Nat. Meth.*, 3:47–53, 2006.

[67] E.J. Gualda, G. Filippidis, G. Voglis, M Mari, C Fotakis, and N. Tavernarakis. In-vivo imaging of cellular structures in caenorhabditis elegans by combined tpef, shg and thg microscopy. *J. Microscopy*, 229:141–150, 2008.

[68] E.J. Gualda, G. Filippidis, M Mari, G. Voglis, M. Vlachos, C Fotakis, and N. Tavernarakis. In vivo imaging of neurodegeneration in caenorhabditis elegans by third harmonic generation microscopy. *J. Microscopy*, 232:270–275, 2008.

[69] J.X. Cheng and X.S. Xie. Coherent anti-stokes raman scattering microscopy: Instrumentation, theory, and applications. *J. Phys. Chem. B*, 108:827–840, 2004.

[70] Michiel Muller and Juleon M. Schins. Imaging the thermodynamic state of lipid membranes with multiplex cars microscopy. *J. Phys. Chem. B*, 106:3715–3723, 2002.

[71] C.L. Evans, E.O. Potma, M. Puoris'haag, D. Cote, C.P. Lin, and X.S. Xie. Chemical imaging of tissue in vivo with video-rate coherent anti-stokes raman scattering microscopy. *Proc. Natl. Acad. Sci. USA*, 102:16807–16812, 2005.

[72] J.X. Cheng, Y.K. Jia, G:F. Zheng, and X.S. Xie. Laser-scanning coherent anti-stokes Raman scattering microscopy and applications to cell biology. *Biophy. J.*, 83(1):502–509, JUL 2002.

[73] H.F. Wang, Y. Fu, P. Zickmund, R.Y. Shi, and J.X. Cheng. Coherent anti-stokes Raman scattering imaging of axonal myelin in live spinal tissues. *Biophy. J.*, 89(1):581–591, JUL 2005.

[74] X.L. Nan, E.O. Potma, and X.S. Xie. Nonperturbative chemical imaging of organelle transport in living cells with coherent anti-stokes Raman scattering microscopy. *Biophy. J*, 91(2):728–735, JUL 15 2006.

[75] Thomas Hellerer, Claes Axaeng, Christian Brackmann, Per Hillertz, Marc Pilon, and Annika Enejder. Monitoring of lipid storage in Caenorhabditis elegans using coherent anti-Stokes Raman scattering (CARS) microscopy. *Proc. Natl. Acad. Sci. USA*, 104(37):14658–14663, SEP 11 2007.

[76] Karsten König, Iris Riemann, Peter Fischer, and Karl-Jrgen Halbhuber. Intracellular nanosurgery with near infrared femtosecond laser pulses. *Cell. Mol. Biol.*, 45:195–201, 1999.

[77] Karsten König, Iris Riemann, and Wolfgang Fritzsche. Nanodissection of human chromosomes n with near infrared femtosecond laser pulses. *Opt. Lett.*, 26:819–821, 2001.

[78] Steven P. Abramow John E. Mancuso. *Laser Surgery: Applications and Techniques.* Saunders, USA, 1992.

[79] Carmen A Puliafito. *Laser Surgery and Medicine: Principles and Practice.* Wiley-Liss, USA, 1992.

[80] Kazuhiko Atsumi. *New Frontiers in Laser Medicine and Surgery.* Elsevier Science Pub. Co., USA, 1983.

[81] Mehmet Fatih Yanik, Hulusi Cinar, Hediye Nese Cinar, Andrew D. Chisholm, Yishi Jin, and Adela Ben-Yakar. Functional regeneration after laser axotomy. *Nature*, 432:822, 2004.

[82] A. Vogel, J. Noack, G. Hiittman, and G. Paltauf. *Laser Ablation and its Applications: Springer Series in Optical Sciences*, chapter 10. Springer, 2006.

[83] A. Vogel, J. Noack1, G. Hüttman1, and G. Paltauf. Mechanisms of femtosecond laser nanosurgery of cells and tissues. *Appl. Phys. B*, 81:1015–1047, 2005.

[84] A. Vogel, J. Noack, G. Hüttman, and G. Paltauf. Mechanisms of femtosecond laser nanosurgery of cells and tissues. *Appl. Phys. B*, 81:1015–1047, 2005.

[85] Nan Shen. *Photodisruption in Biological Tissues Using Femtosecond Laser Pulses.* PhD thesis, Harvard University, 2003.

[86] Andrea B. Huber, Alex L. Kolodkin, David D. Ginty, and Jean-Francois Cloutier. Signaling at the growth cone:ligand-receptor complexes and the control of axon growth and guidance. *Annu. Rev. Neurosci.*, 26:509–563, 2003.

[87] Erik W. Dent and Frank B. Gertler. Cytoskeletal dynamics and transport in growth cone motility and axon guidance. *Neuron*, 40:209–227, 2003.

[88] P. Lamoureux, Z.F. Altun-Gultekin, C. Lin, J.A. Wagner, and S.R. Heidemann. Rac is required for growth cone function but not neurite assembly. *J. Cell. Sci.*, 110:635–641, 1997.

[89] Jeffrey L. Goldberg. How does an axon grow? *Genes & Dev.*, 17:941–958, 2003.

[90] Daniel G. Jay. The clutch hypothesis revisited: Ascribing the roles of actin-associated proteins in filopodial protrusion in the nerve growth cone. *J Neurobiol.*, 44:114–125, 2000.

[91] A.K. Lewis and P.C. Bridgman. Nerve growth cone lamellipodia contain two populations of actin filaments that differ in organization. *J. Cell Biol.*, 119:1219–1243, 1992.

[92] E.W. Dent and K. Kalil. Axon branching requires interactions between dynamic microtubules and actin filaments. *J. Neurosci.*, 21:9757–9769, 2001.

[93] T. Mitchison and M. Kirschner. Cytoskeletal dynamics and nerve growth. *Neuron*, 1:761–772, 1988.

[94] E. Tanaka and J. Sabry. Making the connection: Cytoskeletal rearrangements during growth cone guidance. *Cell*, 83:171–176, 1995.

[95] P. Forscher and S.J. Smith. Actions of cytochalasins on the organization of actin filaments and microtubules in a neuronal growth cone. *J. Cell. Biol.*, 107:1505–1516, 1988.

[96] D.M. Suter, L.D. Errante, V. Belotserkovsky, and P. Forscher. The ig superfamily cell adhesion molecule, apcam, mediates growth cone steering by substrate-cytoskeletal coupling. *J. Cell. Biol.*, 141:227–240, 1998.

[97] C.H. Lin and P. Forscher. Growth cone advance is inversely proportional to retrograde f-actin flow. *Neuron*, 14:763–771, 1995.

[98] Inderbir Singh. *Textbook of Human Neuroanatomy.* Jaypee Brothers, New Delhi, India, 2006.

[99] Y. Li and G. Raisman. Schwann cells induce sprouting in motor and sensory axons in the adult rat spinal cord. *J Neurosci.*, 14:4050–4063, 1994.

[100] C.L. Paino and C. Fernandez-Valle. Regrowth of axons in lesioned adult rat spinal cord: Promotion by implants of cultured schwann cells. *J. Neurocytol.*, 23:433–452, 1994.

[101] Noam Y. Harel and Stephen M. Strittmatter. Can regenerating axons recapitulate developmental guidance during recovery from spinal cord injury? *Nat. Rev. Neurosci.*, 7:603–616, 2006.

[102] Jin Qiu, Dongming Cai, and Marie T. Filbin. Glial inhibition of nerve regeneration in the mature mammalian cns. *GLIA*, 29:166–174, 2000.

[103] L.B. Jakeman and P.J. Reier. Axonal projections between fetal spinal cord transplants and the adult rat spinal cord: a neuroanatomical tracing study of local interactions. *J. Comp. Neurol.*, 307:311–334, 1991.

[104] Colin D. McCaig, Ann M. Rajnicek, Bing Song, and Min Zhao. Has electrical growth cone guidance found its potential? *TRENDS in Neurosciences*, 25:354–359, 2002.

[105] Nilesh Patel and Mu-Ming Poo. Orientation of neurite growth by extracellular electric fields. *J. Neurosci.*, 2:483–496, 1982.

[106] Nilesh Patel and Mu-Ming Poo. Perturbation of the direction of neurite growth by pulsed and focal electric fields. *J. Neurosci.*, 4:2939–2947, 1984.

[107] A.M. Rajnicek *et al.* The direction of neurite growth in a weak dc electric field depends on the substratum: contributions of substrate adhesivity and surface charge. *Dev. Biol.*, 203:412–423, 1998.

[108] R.J. Cork *et al.* The growth of pc12 neurites is biased toward the anode. *J. Neurobiol.*, 25:1609–1616, 1994.

[109] C.D. McCaig. Nerve branching is induced and oriented by a small applied electric field. *J. Cell Sci.*, 95:605–615, 1990.

[110] L. Hinkle *et al.* The direction of growth of differentiating neurones and myoblasts from frog embryos in an applied electric field. *J. Physiol.*, 314:121–135, 1981.

[111] A.M. Rajnicek and C.D. McCaig. camp and protein kinase a signaling underlie growth cone turning in a physiological electric field. *Soc. Neurosci. Abstr.*, 27:795, 2001.

[112] K.S. Fang *et al.* Epidermal growth factor receptor relocalization and kinase activity are necessary for directional migration of keratinocytes in dc electric fields. *J. Cell Sci.*, 112:1967–1978, 1999.

[113] G. Ming *et al.* Electrical activity modulates growth cone guidance by diffusible factors. *Neuron*, 29:441–452, 2001.

[114] C.D. McCaig *et al.* Electrical activity modulates growth cone guidance by diffusible factors. *Dev. Dyn.*, 217:299–308, 2000.

[115] A. Rajnicek, S. Britland, and C. McCaig. Contact guidance of cns neurites on grooved quartz: influence of groove dimensions, neuronal age and cell type. *J. Cell Sci.*, 110:2905–2913, 1997.

[116] Samantha Allison Moore. *Investigations of Laser-Induced Neuronal Guidance.* PhD thesis, The University of Texas at Austin, 2004.

[117] E. Stepien, J. Stanisz, and W. Korohoda. Contact guidance of chick embryo neurons on single scratches in glass and on underlying aligned human skin fibroblasts. *Cell Biol. Int.*, 23:105–116, 1999.

[118] N. Dubey, P.C. Letourneau, and R.T. Tranquillo. Guided neurite elongation and schwann cell invasion into magnetically aligned collagen in simulated peripheral nerve regeneration. *Exp. Neurol.*, 158:338–350, 1999.

[119] P. C. Letourneau N. Dubey and R. T. Tranquillo. Neuronal contact guidance in magnetically aligned fibrin gels: effect of variation in gel mechano-structural properties. *Biomaterials*, 22:1065–1075, 2001.

[120] Matthias Merz and Peter Fromherz. Neuronal contact guidance in magnetically aligned fibrin gels: effect of variation in gel mechano-structural properties. *Adv. Mater.*, 14:141, 2002.

[121] Richard G. Pearson, Yves Molino, Philip M. Williams, Saul J.B. Tendler, Martyn C. Davies, Clive J. Roberts, , and Kevin M. Shakesheff. Spatial confinement of neurite regrowth from dorsal root ganglia within nonporous microconduits. *Tissue. Engg.*, 9:201–208, 2003.

[122] S.L. Rogers, P.C. Letourneau, S. L.Palm, J. McCarthy, and L.T. Furcht. Neurite extension by peripheral and central nervous system neurons in response to substratum-bound fibronectin and laminin. *Dev. Biol.*, 98:212–220, 1983.

[123] J.A. Hammarback, J.B. McCarthy, S.L. Palm, L.T. Furcht, and P.C. Letourneau. rowth cone guidance by substrate-bound laminin pathways is correlated with neuron-to-pathway adhesivity. *Dev. Biol.*, 126:29–39, 1988.

[124] C.D. James, R. Davis M. Meyer, A. Turner, S. Turner, G. Withers, L. Kam, G. Banker, H. Craighead, M. Isaacson, J. Turner, and W. Shain. Aligned microcontact printing of micrometer-scale poly-l-lysine structures for controlled growth of cultured neurons on planar microelectrode arrays. *IEEE Trans. Biomed. Eng.*, 47:17–21, 2000.

[125] A.A. Oliva Jr., C.D. James, C.E. Kingman, H.G. Craighead, and G.A. Banker. Patterning axonal guidance molecules using a novel strategy for microcontact printing. *Neurochem. Res.*, 28:1639–1648, 2003.

[126] G. Gallo, F.B. Lefcort, and P.C. Letourneau. The trka receptor mediates growth cone turning toward a localized source of nerve growth factor. *J. Neurosci.*, 17:5445–5454, 1997.

[127] G. Ming, H. Song, B. Berninger, N. Inagaki, M. Tessier-Lavigne, and M. Poo. Phospholipase c-gamma and phosphoinositide 3-kinase mediate cytoplasmic signaling in nerve growth cone guidance. *Neuron*, 23:139–148, 1999.

[128] G. Gallo and P.C. Letourneau. Neurotrophins and the dynamic regulation of the neuronal cytoskeleton. *J. Neurobiol.*, 44:159–173, 2000.

[129] G. Gallo and P.C. Letourneau. Localized sources of neurotrophins initiate axon collateral sprouting. *J. Neurosci.*, 18:5403–5414, 1998.

[130] J. Dai and M.P. Sheetz. Axon membrane flows from the growth cone to the cell body. *Cell*, 83:693–701, 1995.

[131] J. Zheng, P. Lamoureux, V. Santiago, T. Dennerll, R.E. Buxbaum, and S.R. Heidemann. Tensile regulation of axonal elongation and initiation. *J. Neurosci.*, 11:1117–1125, 1991.

[132] P. Lamoureux, J. Zheng, R.E. Buxbaum, and S.R. Heidemann. A cytomechanical investigation of neurite growth on different culture surfaces. *J. Cell Biol.*, 118:655–661, 1992.

[133] Jing Zheng, Robert E. Buxbaum, and S. R. Heidemann. Measurements of growth cone adhesion to culture surfaces by micromanipulation. *J. Cell Biol.*, 127:2049–2060, 1994.

[134] W.J. Sigurdson and C.E. Morris. Stretch-activated ion channels in growth cones of snail neurons. *J. Neurosci.*, 9:2801–2808, 1989.

[135] J.Q. Zheng. Turning of nerve growth cones induced by localized increases in intracellular calcium ions. *Nature*, 403:89–93, 2000.

[136] Su Cheng, Matthew S. Geddis, and Vincent Rehder. Local calcium changes regulate the length of growth cone filopodia. *J. Neurobiol.*, 50:263–275, 2002.

[137] A. Ehrlicher, T. Betz, B. Hermann, D. Koch, V. Milner, M. G. Raizen, and J. Käs. Guiding neuronal growth with light. *Proc. Natl. Acad .Sci. USA*, 99:16024–16028, 2002.

[138] Samarendra K. Mohanty, Mrinalini Sharma, Mitradas M. Panicker, and Pradeep K. Gupta. Controlled induction, enhancement, and guidance of neuronal growth cones by use of line optical tweezers. *Opt. Lett.*, 30:2596–2598, 2005.

[139] D.J. Stevenson, T.K. Lake, B. Agate, Garcs-Chvez, K. Dholakia, and F. Gunn-Moore. Optically guided neuronal growth at near infrared wavelengths. *Opt. Exp.*, 14:9786–9793, 2006.

[140] D.J. Carnegie, D.J. Stevenson, M. Mazilul, F. Gunn-Moore, and K. Dholakia. Guided neuronal growth using optical line traps. *Opt. Exp.*, 16:10507–10517, 2008.

[141] Timo Betz, Daryl Lim, and Josef A. Käs. Neuronal growth: A bistable stochastic process. *Phy. Rev. Lett.*, 96:098103, 2006.

[142] Jennie P. Mather and David Barnes. *Animal Cell Culture Methods.* Academic Press, USA, 1998.

[143] Kevin Strange. C. elegans *Methods and Applications.* Humana Press, USA, 2006.

[144] *http://www.wormatlas.org/handbook/anatomyintro/anatomyintro.htm.*

[145] *http://www.wormatlas.org/handbook/mesodermal.htm/musclepartI.htm.*

[146] *http://www.wormatlas.org/handbook/mesodermal.htm/musclepartII.htm.*

[147] *http://www.wormatlas.org/handbook/mesodermal.htm/musclepartIII.htm.*

[148] ERIC AAMODT. *The Neurobiology of* C. elegans. ACADEMIC PRESS, Amsterdam, 2006.

[149] *http://www.wormbook.org/chapters/www_strainmaintain/strainmaintain.html.*

[150] S. Ramn y Cajal. *Textura del Sistema Nervioso del Hombre y los Vertebrados.* Spain, 1904.

[151] M. Tessier-Lavigne and C.S. Goodman. The molecular biology of axon guidance. *Science*, 274:1123–1133, 1996.

[152] E.R Kandel, J.H. Schwartz, and T.M. Jessell. *Principles of Neural Science, 4th ed.* McGraw-Hill, New York, 2000.

[153] D. Pantaloni, C. Le Clainche, and M.F. Carlier. Mechanism of actin-based motility. *Science*, 292:1502–1506, 2001.

[154] D.M. Suter and P.Forscher. Substrate-cytoskeletal coupling as a mechanism for the regulation of growth cone motility and guidance. *J. Neurobiol.*, 44:97–113, 2000.

[155] G.G. Borisy and T.M. Svitkina. Actin machinery: pushing the envelope. *Curr. Opin. Cell Biol.*, 12:104–112, 2000.

[156] B.J. Dickson. Molecular mechanisms of axon guidance. *Science*, 298:1959–1964, 2002.

[157] Y. Naka, A. Eda, H. Takei, and N. Shimizu. Neurite outgrowths of neurons using neurotropin-coated nano-scale magnetic beads. *J. Biosci. Bioeng.*, 98:348–352, 2004.

[158] P. Fromherz, H. Schaden, and T. Vetter. Guided outgrowth of leech neurons in culture. *Neurosci. Lett.*, 129:77–80, 1991.

[159] J.W. Lee, K.S. Lee, N. Cho, B.K. Ju, K.B. Lee, and S.H. Lee. Topographical guidance of mouse neuronal cell on sio(2) microtracks. *Sensor. Actuat. B-Chem.*, 128:252–257, 2007.

[160] B. Kaehr, R. Allen, D.J. Javier, J. Currie, and J.B. Shear. Guiding neuronal development with in situ microfabrication. *Proc. Natal. Acad. Sci.*, 46:16104–16108, 2004.

[161] T.M. Fischer, P.N. Steinmetz, and D.J. Odde. Robust micromechanical neurite elicitation in synapse-competent neurons via magnetic bead force application. *Ann. Biomed. Eng.*, 33:1229–1237, 2005.

[162] Akon Higuchi, Toru Watanabe, Yusuke Noguchi, Yung Chang, Wen-Yih Chen, and Yuki Matsuoka. Visible light regulates neurite outgrowth of nerve cells. *Cytotechnology*, 54:181–188, 2007.

[163] K.D. Desmet, D.A. Paz, J.J. Corry, J.T. Eells, M.T.T. Wong-Riley, M.M. Henry, E.V. Buchmann, M.P. Connelly, J.V. Dovi, H.L. Liang, D.S. Henshel, R.L. Yeager, D.S. Millsap, J. Lim, L.J. Gould, R. Das, M. Jett, B.D. Hodgson, D. Margolis, and H.T. Whelan. Clinical and experimental applications of nir-led photobiomodulation. *Photomed. Laser Surg.*, 24:121–128, 2006.

[164] M.T.T. Wong-Riley, H.L. Liang, J.T. Eells, B. Chance, M.M. Henry, E. Buchmann, M. Kane, and H.T. Whelan. Photobiomodulation directly benefits primary neurons functionally inactivated by toxins: Role of cytochrome c oxidase. *J. Biol. Chem.*, 280:4761–4771, 2005.

[165] A.P. Sommer, A.L.B. Pinheiro, A.R. Mester, R.P. Franke, and H.T. Whelan. Biostimulatory windows in lowintensity laser activation: lasers, scanners, and nasa's light emitting diode array system. *J. Clin. Laser Med. Surg.*, 19:29–33, 2001.

[166] A.W. Henkel, I. Upmann, C.R. Bartl, D. Bnsch, C. Reichardt, J.M. Maler, R. Umsttter M. Nrnberger, U. Reulbach, J. Kornhuber, and J. Wiltfang. Light-induced exocytosis in cell development and differentiation. *J. Cel. Biochem.*, 97:1393–1406, 2006.

[167] T. Kumbalasiria and I. Provencio. Melanopsin and other novel mammalian opsins. *Exp. Eye Res.*, 81:368–375, 2005.

[168] G. Albrecht-Buehler. Surface extension of 3t3 cells towards distant infrared light sources. *J. Cell. Biol.*, 114:493–502, 1991.

[169] G. Albrecht-Buehler. Changes of cell behavior by near infrared signals. *Cell Mot. Cytoskel.*, 32:299–304, 1995.

[170] G. Albrecht-Buehler. A long-range attraction between aggregating 3t3 cells mediated by near-infrared light scattering. *Proc. Natal. Acad. Sci.*, 102:5050–5055, 2005.

[171] A.K.N. Thayil, E.J. Gualda, S. Psilodimitrakopoulos, I.G. Cormack, M. Mathew I. Amat-Roldn, D. Artigas, and P. Loza-Alvarez. Starch-based backwards shg for in-situ mefisto pulse characterization in multiphoton microscopy. *J. Microsc.*, 230:70–75, 2008.

[172] G. Albrecht-Buehler. Rudimentary form of cellular "vision". *Proc. Natal. Acad. Sci.*, 89:8288–8292, 1992.

[173] H.J. Niggli. Ultraweak photons emitted by cells: Biophotons. *J Photochem Photobiol. B*, 14:144–146, 1992.

[174] H.J. Niggli, C. Scaletta, Y. Yu, F.A. Popp, and L.A. Applegate. Ultraweak photon emission in assessing bone growth factor efficiency using fibroblastic differentiation. *J Photochem Photobiol. B*, 64:62–68, 2001.

[175] M.V. Trushin. Light mediated conversation among microorganisms. *Microbiol. Res.*, 159:01–10, 2004.

[176] M.V. Trushin. Studies on distant regulation of bacterial growth and light emission. *Microbiology*, 149:363–368, 2003.

[177] A. Farhadi, C.Forsyth, A. Banan, M. Shaikh, P. Engen, J.Z. Fields, and A. Keshavarzian. Evidence for non-chemical, non-electrical intercellular signaling in intestinal epithelial cells. *Bioelectrochemistry*, 71:142–148, 2007.

[178] G. Albrecht-Buehler. Cellular infrared detector appears to be contained in the centrosome. *Cell Mot. Cytoskel.*, 27:262–271, 1994.

[179] G. Albrecht-Buehler. Altered drug resistance of microtubules in cells exposed to infrared light pulses: Are microtubules the nerves of cells? *Cell Mot. Cytoskel.*, 40:183–192, 1998.

[180] T. Kodama, M.R. Hamblin, and A.G. Doukas. Cytoplasmic molecular delivery with shock waves: Importance of impulse. *Biophys. J.*, 79:1821–1832, 2000.

[181] A.G. Doukas and T.J. Flotte. Physical characteristics and biological effects of laser-induced stress waves. *Ultrasound Med. Biol.*, 22:151–164, 1996.

[182] E.N. Glezer, C.B. Schaffer, N.Nishimura, and E.Mazur. Minimally disruptive laser-induced breakdown in water. *Opt. Lett.*, 22:1817–1819, 1997.

[183] P.A. Benedetti. From the histophotometer to the confocal microscope: the evolution of analytical microscopy. *Eur. J. Histochem.*, 42:Spec No:11–7, 1998.

[184] P. Stoller, K.M. Reiser, P.M. Celliers, , and A. M. Rubenchik. Polarization-modulated second harmonic generation in collagen. *Biophys. J.*, 82:3330–3342, 2002.

[185] B.G. Wang, I. Riemann, H. Schubert, D. Schweitzer, K. Konig, and K. J. Halbhuber. Multiphoton microscopy for monitoring intratissue femtosecond laser surgery effects. *Biophys. J.*, 39:527–533, 2007.

[186] A. K. N. Thayil, I. G. Cormack, A. Pereira, E. M. Blanco, M. Mathew, D. Artigas, and P. Loza-Alvarez. Decrease in laser ablation threshold for epithelial tissue microsurgery in a living drosophila embryo during dorsal closure. *J. Microsc.*, 232:362–368, 2008.

[187] *http://www.nikoninstruments.com/c1si/.*

[188] A. Ridsdale, I. Micu, and P. K. Stys. Conversion of the nikon c1 confocal laser-scanning head for multiphoton excitation on an upright microscope. *App. Opt.*, 43:1669–1675, 2004.

[189] K. König, U. Simon, and K.J. Halbhuber. 3d resolved two-photon fluorescence microscopy of living cells using a modified confocal laser scanning microscope. *Cell. Mol. Biol.*, 42:1181–1194, 1996.

[190] A. Diaspro, M. Corosu, P. Ramoino, and M. Robello. Adapting a compact confocal microscope system to a two-photon excitation fluorescence imaging architecture. *Microsc. Res. Techniq.*, 47:196–205, 1999.

[191] A. Majewska, G. Yiu, and R. Yuste. A custom-made two-photon microscope and deconvolution system. *Eur. J. Physiol.*, 441:398–408, 2000.

[192] V. Nikolenko, B. Nemet, and R. Yuste. A two-photon and second-harmonic microscope. *Methods*, 3:3–15, 2003.

[193] *http://www.zeiss.com/c12567be0045acf1/Contents-Frame/86b98821993159 75c125709f003e8f07.*

[194] *http://www.olympusamerica.com/seg_section/product.asp?product=1020.*

[195] M. Goksör, J. Enger, and D. Hanstorp. Optical manipulation in combination with multiphoton microscopy for single-cell studies. *Appl. Opt.*, 43:4831–4837, 2004.

[196] T.B. Huff, Y. Shi, Y. Fu, H. Wang, and J.X. Cheng. Multimodal nonlinear optical microscopy and applications to central nervous system imaging. *IEEE J. Sel. Top. Quant.*, 14:4–9, 2008.

[197] P. S. Tsai, N. Nishimura, E. J. Yoder, A. White, E. Dolnick, and D. Kleinfeld. *Methods for In Vivo Optical Imaging*, pages 113–171. CRC Press, USA, 2002.

[198] *http://www.nikoninstruments.com/ti/.*

[199] S. Brenner. The genetics of caenorhabditis elegans. *Genetics*, 77:71–94, 1974.

[200] H. Yoo, I. Song, and D.G. Gweon. Measurement and restoration of the point spread function of fluorescence confocal microscopy. *J. Microsc*, 221:172–176, 2006.

[201] Alan W. Bigelow, Charles R. Geard, Gerhard Randers-Pehrson, and David J. Brenner. Microbeam-integrated multiphoton imaging system. *Rev. Sci. Instrum.*, 79:123707, 2008.

[202] Samuel H Chung, Damon A Clark, Christopher V Gabel, Eric Mazur, and Aravinthan DT Samuel. The role of the afd neuron in *C. elegans* thermotaxis analyzed using femtosecond laser ablation. *BMC Neuroscience*, 7:30(1)–30(11), 2006.

[203] Hajime Hirase, Volodymyr Nikolenko, Jesse H. Goldberg, and Rafael Yuste. Multiphoton stimulation of neurons. *J. Neurobiol.*, 51:237–247, 2002.

[204] M. Callaway and Rafael Yuste. Stimulating neurons with light. *Curr. Opin. Neurobiol.*, 12:587–592, 2002.

[205] L. Sacconi, I. M. Tolic-Nrrelykke, F. Vanzi M. D'Amico, M. Olivotto, R. Antolini, and F. S. Pavone. Cell imaging and manipulation by nonlinear optical microscopy. *Cell Biochem. Biophys.*, 45:289–302, 2006.

[206] G. Volpe, G.P. Singh, and D. Petrov. Dynamics of a growing cell in an optical trap. *Appl. Phys.Lett.*, 88:231106–231109, 2006.

[207] G. Volpe, G. Volpe, and D. Petrov. Brownian motion in a nonhomogeneous force field and photonic force microscope. *Phys. Rev. E*, 76:061118–0611117, 2007.

[208] L. Paterson, B. Agate, M. Comrie, R. Ferguson, T. K. Lake, J. E. Morris, A. E. Carruthers, C. T. A. Brown, W. Sibbett, P. E. Bryant, F. Gunn-Moore, A. C. Riches, and K. Dholakia. Photoporation and cell transfection using a violet diode laser. *Opt. Express.*, 13:595–600, 2005.

[209] C.M. Creely, G. Volpe, G. P. Singh, M. Soler, and D.V. Petrov. Raman imaging of floating cells. *Opt. Express.*, 12:6105–6110, 2005.

[210] E. J. Gualda, G. Filippidis, G. Voglis, M. Mari, C. Fotakis, and N. Tavernarakis. In vivo imaging of anatomical features of the nematode Caenorhabditis elegans using non-linear (TPEF-SHG-THG) microscopy - art. no. 663003. In *Confocal, Multiphoton, and Nonlinear Microscopic Imaging III*, volume 6630 of *Proc. SPIE*, page 63003, 2007.

[211] Willy Supatto, Delphine Débarre, Bruno Moulia, Eric Brouzs, Jean-Louis Martin, Emmanuel Farge, and Emmanuel Beaurepaire. In vivo modulation of morphogenetic movements in drosophila embryos with femtosecond laser pulses. *Proc. Natl. Acad. Sci. USA*, 102:1047–1052, 2005.

[212] S. Kumar, I. Z. Maxwell, A. Heisterkamp, T. R. Polte, T. P. Lele, M. Salanga, E. Mazur, and D. E. Ingber. Viscoelastic retraction of single living stress fibers and its impact on cell shape, cytoskeletal organization,and extracellular matrix mechanics. *Biophys. J.*, 90:3762–3773, 2006.

[213] T. Shimada, W. Watanabe, S. Matsunaga, T. Higashi, H. Ishii, K. Fukui, K. Isobe, and K. Itoh. Intracellular disruption of mitochondria in a living hela cell with a 76-mhz femtosecond laser oscillator. *Opt. Express*, 13:9869–9880, 2005.

[214] N. Nishimura, C. B. Schaffer, B. Friedman, P. S. Tsai, P. D. Lyden, and D. Kleinfeld. Targeted insult to subsurface cortical blood vessels using ultrashort laser pulses: three models of stroke. *Nat. Methods*, 3:99–108, 2006.

[215] A. Heisterkamp, T. Ripken, T. Mamom, W. Drommer, H.Welling, W. Ertmer, , and H. Lubatschowski. Nonlinear side effects of fs pulses inside corneal tissue during photodisruption. *Appl. Phys B-Lasers Opt.*, 74:419–425, 2002.

[216] Frederic Bourgeois and Adela Ben-Yakar. Femtosecond laser nanoaxotomy properties and their effect on axonal recovery in c. elegans. *Optics Express*, 15:8521– 8531, 2003.

[217] Samuel X Guo, Frederic Bourgeois, Trushal Chokshi, Nicholas J Durr, Massimo A Hilliard, Nikos Chronis, and Adela Ben-Yakar. Femtosecond laser nanoaxotomy lab-on-a-chip for *in vivo* nerve regeneration. *Nat. Meth.*, 5:531–533, 2008.

[218] C.I. Bargmann and L. Avery. *Laser killing of cells in Caenorhabditis elegans. In Caenorhabditis elegans: Modern Biological Analysis of an Organism*, pages 225–250. Academic Press, USA, 1995.

[219] Zilu Wu, Anindya Ghosh-Roy, Mehmet Fatih Yanik, Jin Z. Zhang, Yishi Jin, and Andrew D. Chisholm. Caenorhabditis elegans neuronal regeneration is influenced by life stage, ephrin signaling, and synaptic branching. *Proc. Natl Acad. Sci. USA*, 104:15132–15137, 2007.

[220] Christopher V. Gabel, Harrison Gabel, Albert Kao Dmitri Pavlichin, Damon A. Clark, and Aravinthan D. T. Samuel. Neural circuits mediate electrosensory behavior in caenorhabditis elegans. *J. Neurosci.*, 27:7586–7596, 2007.

[221] Damon A. Clark, David Biron, Piali Sengupta, and Aravinthan D. T. Samuel. The afd sensory neurons encode multiple functions underlying thermotactic behavior in caenorhabditis elegans. *J. Neurosci.*, 26:7444–7451, 2006.

[222] Damon A. Clark, Christopher V. Gabel, Timothy M. Lee, and Aravinthan D. T. Samuel. Short-term adaptation and temporal processing in the cryophilic response of caenorhabditis elegans. *J. Neurophysiol.*, 97:1903–1910, 2007.

[223] S. J. Dixon and P. J. Roy. Muscle arm development in caenorhabditis elegans. *Development*, 132:3079–3092, 2005.

[224] M.D. Abramoff, P.J. Magelhaes, and S.J. Ram. Image processing with imagej. *Biophotonics International*, 11:36–42, 2004.

[225] N. I. Smith, Y. Kumamoto, S. Iwanaga, J. Ando, K. Fujita, and S. Kawata. A femtosecond laser pacemaker for heart muscle cells. *Opt. Express*, 16:8604–8616, 2008.

[226] S. Psilodimitrakopoulos, S. I. C. O. Santos, I. Amat-Roldan, A. K. N. Thayil, D. Artigas, and P. Loza-Alvarez. In vivo, pixel-resolution mapping of thick filaments' orientation in nonfibrilar muscle using polarization-sensitive second harmonic generation microscopy. *J. Biomed. Opt.*, 14:014001, 2009.

[227] M. C. Hogan, C. M. Stary, R. S. Balaban, and C. A. Combs. Nad(p)h fluorescence imaging of mitochondrial metabolism in contracting xenopus skeletal muscle fibers: effect of oxygen availability. *Appl. Physiol.*, 98:1420–1426, 2005.

[228] Catarina Mrck, Claes Axng, and Marc Pilon. A genetic analysis of axon guidance in the *C.elegans* pharynx. *Dev. Biol.*, 260:158–175, 2003.

[229] J.H.Thomas, M.J. Stern, and H.R. Horvitz. Cell interactions coordinate the development of the *C.elegans* egg-laying system. *Cell*, 62:1041–1052, 1990.

[230] E.M. Hedgecock, J.G. Culotti, D.H. Hall, and B.D. Stern. Genetics of cell and axon migrations in caenorhabditis elegans. *Development*, 100:365–382, 1987.

[231] T.Q. Nguyen, H.Sawa, H. Okano, and J.G. White. The c.elegans septin genes, unc-59 and unc-61, are required for normal postembryonic cytokineses and morphogenesis but have no essential function in embryogenesis. *J. Cell Sci.*, 113:3825–3837, 2000.

[232] C. Axäng, M. Rauthan, D. H. Hall, and M. Pilon. The twisted pharynx phenotype in *C.elegans*. *BMC Dev. Biol.*, 7:61(1)–61(13), 2007.

[233] T.A. Brown. *Gene Cloning and DNA analysis*. Blackwell Publishing, UK, 2000.

[234] J. Sambrook and D. Russell. *Molecular Cloning, A Laboratory Manual*. CSHL press, USA, 2000.

[235] Irina A. Kramerova, Nobuko Kawaguchi, Liselotte I. Fessler, Robert E. Nelson, Yali Chen, Andrei A. Kramerov, Marion Kusche-Gullberg, James M. Kramer, Brian D. Ackley, Aleksander L. Sieron, Darwin J. Prockop, and John H. Fessler. Papilin in development; a pericellular protein with a homology to the adamts metalloproteinases. *Development*, 127:5475–5485, 2000.

[236] Irina A. Kramerova, Andrei A. Kramerov, and John H. Fessler. Alternative splicing of papilin and the diversity of drosophila extracellular matrix during embryonic morphogenesis. *Dev. Dyn.*, 226:634–642, 2003.

[237] Takehiro Kawano, Hong Zheng, David C. Merz, Yuji Kohara, Katsuyuki K. Tamai, Kiyoji Nishiwaki, and Joseph G. Culotti. C. elegans mig-6 encodes papilin isoforms that affect distinct aspects of dtc migration, and interacts genetically with mig-17 and collagen iv. *Dev. Dyn.*, 136:1433–1442, 2009.

[238] A. Chisholm and M. Tessier-Lavigne. Gonservation and divergence of axon guidance mechanisms. *Curr. Opin. Neurobiol.*, 9:603–615, 1999.

[239] J. Raper. Semaphorins and their receptors in vertebrates and invertebrates. *Curr. Opin. Neurobiol.*, 10:88–94, 2000.

[240] M. Tessier-Lavigne S. He. Molecular basis of axonal chemorepulsion: Neuropilin is a semaphorin/collapsin receptor. *Cell*, 90:739–751, 1997.

[241] C.J.Harrison T. Cutforth. Ephs and ephrins close ranks. *Trends Neurosci.*, 25:332–334, 2002.

[242] K. Kullander and R. Klein. Mechanisms and functions of eph and ephrin signalling. *Nat.Rev. Mol. Cell Biol.*, 3:475–486, 2002.

[243] C.J. Desai, N.X. Krueger, H. Saito, and K. Zinn. Competition and cooperation among receptor tyrosine phosphatases control motoneuron growth cone guidance in drosophila. *Development*, 124:1941–1952, 1997.

[244] L.F. Reichardt E.J. Huang. Neurotrophins:roles in neuronal development and function. *Annu. Rev. Neurosci.*, 24:677–736, 2001.

[245] S.D. Skaper, S.E. Moore, and F.S. Walsh. Cell signalling cascades regulating neuronal growth-promoting and inhibitory cues. *Prog.Neurobiol.*, 65:593–608, 2001.

Appendix A

Neuroscience

A.1 Axon guidance cues

A.1.1 Rho GTPases

Rho family GTPases orchestrate actin filament assembly and disassembly through the control of actin polymerization, branching, and depolymerization. Moreover, Rho family members direct actin-myosin-dependent contractility, controlling the retrograde flow of F-actin within the growth cone. The best studied Rho GTPases, Cdc42, Rac, and RhoA, have been implicated in the control of lamellipodial and filopodial dynamics. Rho GTPases cycle between active and inactive states through the binding of guanine nucleotides. In their GTP-bound states, Rho GTPases recruit effector proteins to the membrane and are thus considered active. Hydrolysis of GTP to GDP by their intrinsic GTPase activity disrupts GTPase binding to effectors and thereby inactivates these GTPases. The activity of Rho GTPases is controlled by the opposing actions of guanine nucleotide exchange factors (GEFs) and GTPase activating proteins (GAPs). GEFs facilitate the exchange of GDP to GTP, thereby turning on Rho GTPase signaling, whereas GAPs turn off Rho GTPase signaling by activating their endogenous GTPase activities. Axon guidance receptors can be directly or indirectly coupled to GEFs and GAPs, affording these receptors direct control over Rho GTPases [93].

A.1.2 Netrins

The netrins are a small family of phylogenetically conserved secreted proteins with amino acid sequence similarity to proteins of the laminin family. Netrins function as both neuronal chemoattractants and repellents [238]. An example of netrin bifunctionality is observed in vertebrates, where netrin-1 functions *in-vitro* and *in-vivo* to attract spinal cord commissural neuron axons to the floor plate and in vitro to repel trochlear motor axons. Members of the DCC family of netrin receptors mediate netrin attraction. DCC proteins have large extracellular domains composed of multiple immunoglobulin (Ig) repeats, fibronectin type III (FNIII) repeats, and large cytoplasmic domains with three conserved motifs (P1, P2, and P3). Ligand-gated multimerization of DCC proteins through their P3 regions is required for netrin induced attraction events [93]. A direct association between the DCC and UNC-5 cytoplasmic domains leads to repulsive guidance events [93].

A.1.3 Slits

Members of the Slit family of axon guidance molecules control a wide range of physiological processes during neural development including axon pathfinding axonal and dendritic branching and neuronal cell migration [93]. Slits have been most extensively characterized with respect to their role in orchestrating axonal navigation at the CNS midline. The Robo family of transmembrane proteins includes members that function as receptors for Slits. Abelson (Abl) tyrosine kinase and one of its substrates, Ena, are involved in the Robo signaling cascade. Ena may enhance F-actin polymerization at the leading edge of the growth cone [93].

A.1.4 Semaphorins

The semaphorins belong to a large family of phylogenetically conserved secreted and membrane-associated proteins, members of which are capable of mediating both repulsive and attractive axon guidance events during neural development [239]. More than 30 semaphorins have been identified and all share a conserved N-terminal Sema domain and can be classified into eight subfamilies depending on their structural similarities and species of origin. The plexins, a large family of evolutionarily conserved transmembrane proteins, are essential signal transducing components of most semaphorin receptor complexes [93]. Plexins cannot bind secreted class 3 semaphorins directly, but plexin-A receptors form a complex with the neuropilin proteins, neuropilin-1 (Npn-1) or Npn-2, which function as obligate coreceptors and bind to class 3 semaphorins with high afinity [240]. The Rho family of GTPases appears to provide a critical link between semaphorin receptors and the actin cytoskeleton.

A.1.5 Ephrins

Eph tyrosine kinases, receptors for the ephrins, are encoded by the largest family of receptor tyrosine kinase (RTK) genes in the mammalian genome. These receptors are divided in two subclasses, EphA receptors (EphA1-EphA8), which bind the GPI-linked ephrin-As (ephrinA1-ephrinA5), and EphB receptors (EphB1-EphB6), which bind to transmembrane ephrin-Bs (ephrinB1-ephrinB3) [241]. Ephrin/Eph complexes transduce signals bidirectionally into both receptor (Eph) expressing cells and ligand (ephrin) expressing cells in what is known as “forward” and “reverse” signaling, respectively. There is ample evidence to indicate that both forward and reverse modes of Ephrin-Eph signaling are critical for axon guidance during neural development [242]. Upon ligand engagement Eph receptors undergo autophosphorylation in a manner similar to other RTKs.

A.1.6 Receptor Protein Tyrosine Phosphatases

Members of the large family of protein tyrosine phosphatases (PTPs), have emerged as key regulators of axon growth and guidance. The most compelling case for a role of RPTPs in axon guidance has been made in Drosophila, where the molecules DPTP69D and DLAR have been implicated in both the guidance of motor neuron axons [243]. Moreover, mammalian RPTPδ, RPTPκ, and RPTPμ and chick PTPσ have been implicated in the growth and guidance of several populations of developing vertebrate neurons [93].

A.1.7 Neurotropins

The neurotrophin (NT) family is comprised of nerve growth factor (NGF), BDNF, NT-3, and NT-4. These factors play critical roles in the establishment and maintenance of the nervous system as well as in plasticity in the adult [244]. Neurotrophins are powerful modulators of growth cone steering in vitro. Although p75 was the first identified neurotrophin receptor, members of the Trk family of receptor tyrosine kinases have received the most attention as signaling receptors for the neurotrophins [93]. Like most receptor tyrosine kinases, initiation of signaling through Trks is triggered by ligand-dependent receptor dimerization and trans-phosphorylation of the cytoplasmic domains leading to recruitment of SH2 and PTB domain-containing adapter and effector proteins.

A.1.8 Cell-Adhesion Receptors

Cell-adhesion receptors, including Ig cell-adhesion molecules (CAMs), cadherins, and integrins, direct axon guidance events and many additional developmental processes through interactions with ligands present in the extracellular matrix (ECM) or on neighboring cells [93]. Engagement of all three families of cell-adhesion receptors activates several signaling pathways, including MAPK cascades. Stimulation of NCAM, L1, and N-cadherin through homophilic binding in trans leads to phosphorylation and activation of the FGF receptor tyrosine kinase (FGFR), which triggers a signaling cascade involving PLC, DAG lipase, production of arachidonic acid, increases intracellular calcium levels, and subsequent activation of MAPK signaling [245].

A.1.9 Myelin-Associated Inhibitors: Nogo, MAG, OMgp

The recent identification and characterization of neurite growth-inhibitory molecules associated with myelin and oligodendrocytes provides insight into the mechanisms that prevent axonal regeneration in the adult mammalian system. Although these molecules have mostly been studied in the context of their ability to inhibit regeneration, their expression in the CNS and PNS during neural development suggests they may also play a role in the growth and guidance of axons.

Appendix B

Neuron Culture Protocols

B.1 Dissection Media

Phosphate Buffered Saline (PBS) 1X	500ml
KCl Powder	0.15gr
D-Glucose Powder	1gr
NaH2Co3	275μl
Phenol Red	250μl
Miliq Water	40ml

1. Add KCl powder, Glucose powder and Phenol red in 40ml MiliQ water and mix throughly
2. Filter the solution using 0.2μm pore size filter and add to the PBS
3. Add NaH2Co3 directly to the PBS solution
4. Mix well

B.2 Neurobasal Media for cerebral cortex neurons

Neurobasal Solution	50ml
Normal Horse Serum (NHS)	2.5ml
Glutamine	1.25ml
NaH2Co3	260μl
Penicillin-Streptomycin Solution	500μl
B27	1ml
D-Glucose Liquid	660μl

Appendix C

C.elegans Culture Protocols

C.1 Nematode Growth Media

NaCl	3gr
Bacto Agar	17gr
Bacto Peptone	5gr
1M CaCl2	1ml
1M PPB	25ml
5mg/ml Cholesterol in Ethanol	1ml
1M MgSO4	1ml
Fungizone	0.4μl
Miliq water	972ml
Total	1000ml

1. Make 100ml PPB (pH 6.0) by mixing 13.2ml of 1MK2HPO4 with 86.8ml of 1M KH2PO4

2. Mix NaCl, agar and peptone in a 1 liter bottle and add 972ml of MiliQ water and autoclave

3. Cool the bottle in a 55^0 water bath for 20min

4. Add CaCl2, MgSO4, PPB, cjolesterol and fungizone and mix throughly

5. Using sterile procedures dispense the NGM solution into petri plates.

6. Leave the plates overnight at room temperature.

C.2 Luria Broth for Bacterial Culture

Yeast Extract	5gr
Tryptone	10gr
NaOH	2 pellets
NaCl	5gr
Bacto Agar	15gr
MiliQ Water	1000ml
Total	1000ml

1. Autoclave the solution for atleast 30mins and cool to 55^0C in a water bath.
2. For liquid LB cultures avoid the use of bacto agar.
3. For making LB plates pour the 55^0C solution into petri plates and allow to cool at room temperature.
4. Bacteria (E.coli OP50) can be streaked from another plate onto the new plate and left overnight at room-temperature.
5. Liquid bactrial suspensions can be obtained by seeding a colony of bacteria form a plate into 10ml of LB liquid in a 100ml tube and leaving the tubes overnight in a shaking incubator at 375^0C.

C.3 Freezing Protocol

1. Dissolve NaCl (0.585g), KH2PO4 (0.68g), glycerol (30g), 1M NaOH (0.56ml) in a final volume of 100ml distilled water.
2. Autoclave and allow to cool
3. Add 0.3ml of 0.1M MgSO4 and mix
4. Add 100ml of M9 buffer and mix
5. This is the final 1X freezing solution and can be keppt at room temp for several months.

C.3.1 M9 Protocol

KH2PO4	3gr
NaH2PO4	6gr
NaCl	5gr

Dissolve in distilled water and adjust volume to 1L. Sterilize by autoclaving. Allow to cool and then add 1ml of sterile 1M MgSO4.

Appendix D

Nano-Neurosurgery Appendix

Table D.1: Case by case report of the various collateral damage effects during the process of Nano-neurosurgery detected using various microscopic techniques. CF: Confocal Fluorescence Microscopy; 2PE: Two Photon Excited Fluorescence Microscopy; MLSBF: Multiphoton Laser Scanning Bright Field Imaging; CLSBF: Confocal Laser Scanning Bright Field Imaging; Y:yes; n:no; na: not available; afterZ: damage detected only after changing the focal position; chgSHG: no damage but a change in SHG signal.

Sl: No:	Axon Severed	Induced Autofluorescence (CF)	Induced Autofluorescence (2PE)	Cuticle Damage (MLSBF)	Muscle Damage (SHG)	Cuticle Damage (CLSBF)
1	y	y	y	na	y	na
2	y	y	y	na	y	na
3	Y	n	n	na	Y	na
4	y	n	n	na	n	na
5	y	y	y	na	Y	na
6	na	y	y	y	y	y
7	y	n	n	n	n	n
8	y	n	y	n	n	n
9	y	n	y	tiny	na	n
10	y	y	n	n	na	y
11	n	y	y	n	tiny	y
12	y	y	y	n	y	y
13	y	y	n	n	tiny	n
14	n	y	y	n	tiny	n
15	y	y	y	n	n	n

Continued on next page

Table D.1 – continued from previous page

Sl: No:	Axon Severed	Induced Autofluorescence (CF)	Induced Autofluorescence (2PE)	Cuticle Damage (MLSBF)	Muscle Damage (SHG)	Cuticle Damage (CLSBF)
16	y	n	tiny	n	n	n
17	n	y	y	n	n	n
18	y	n	n	n	y	n
19	n	y	n	na	na	na
20	y	y	n	n	na	n
21	y	n	n	n	n	n
22	y	y	n	n	tiny	n
23	y	y	y	y	y	y
24	y	tiny	y	y	y	n
25	y	n	n	n	tiny	n
26	y	n	n	n	tiny	n
27	y	n	tiny	n	tiny	n
28	y	n	tiny	tiny	tiny	n
29	y	n	n	n	n	n
30	y	n	n	n	n	n
31	y	n	n	n	n	n
32	n	n	n	na	n	n
33	y	n	yes	n	y	n
34	y	n	n	n	n	n
35	y	y	y	n	y	n
36	y	n	y	tiny	tiny	n
37	y	n	y	n	n	n
38	y	n	n	n	tiny	n
39	y	n	yes	n	n	n

Continued on next page

Table D.1 – continued from previous page

Sl: No:	Axon Severed	Induced Autoflu-orescence (CF)	Induced Autoflu-orescence (2PE)	Cuticle Damage (MLSBF)	Muscle Damage (SHG)	Cuticle Damage (CLSBF)
40	y	y	n	n	tiny	n
41	y	n	n	tiny	tiny	n
42	y	n	n	tiny	tiny	n
43	y	n	n	n	n	n
44	y	n	n	n	tiny	n
45	y	n	n	n	tiny	n
46	y	n	n	n	tiny	n
47	y	n	n	n	afterZ	n
48	y	y	y	n	chgSHG	n
49	y	n	y	n	afterZ	n
50	y	n	n	n	n	n
51	y	n	n	n	n	n
52	y	n	n	n	n	n

Appendix E

Molecular Biology Protocols

E.1 Single worm lysis buffer

1M KCl	500μl
1M MgCl2	25μl
M Tris, pH 8.3	100μl
10% NP-40	450μl
10% Tween 20	450μl
0.1% gelatin	1000μl
Water	7475μl
Total	10ml

E.2 PCR reaction master mix

Water	33μll
Pfu Buffer	5μl
dNTPs	1.25μl
Pfu Enzyme	1.5μl
Primer L	2μl
Primer R	2μl
Total	40.75μl

E.3 Topo-isomerization protocol

E.3.1 Preparing Cloning Mix

1. Mix 4μl of insert, 1μl of salt solution and 1μl of pCR®II Blunt Topo
2. Incubate 5 min at room temperature
3. Place on ice

E.3.2 Transformation of one shot competent cells

1. Thaw the competent cells on ice

2. Add 2μl of cloning mix.
3. Incubate on ice 15mins.
4. Heat Shock 30sec at 420C
5. Transfer to ice
6. Add 250μl of soc solution at room temperature
7. Cap tightly and shake horizontally at 370C for 1 hour
8. Plate 25μl and 250μl on 50μg/ml kanamycin plates